

A functional operon delineates an extracellular pathway that controls body asymmetry only in animals with a ciliated left-right organizer

Emmanuelle Szenker-Ravi, Tim Ott, Muznah Khatoo, Anne Moreau de Bellaing, Wei Xuan Goh, Yan Ling Chong, Anja Beckers, Darshini Kannesan, Guillaume Louvel, Priyanka Anujan, et al.

▶ To cite this version:

Emmanuelle Szenker-Ravi, Tim Ott, Muznah Khatoo, Anne Moreau de Bellaing, Wei Xuan Goh, et al.. A functional operon delineates an extracellular pathway that controls body asymmetry only in animals with a ciliated left-right organizer. Nature Genetics, 2022, 54 (1), pp.62-72. 10.1038/s41588-021-00970-4. hal-03876795

HAL Id: hal-03876795 https://hal.science/hal-03876795

Submitted on 28 Nov 2022

HAL is a multi-disciplinary open access archive for the deposit and dissemination of scientific research documents, whether they are published or not. The documents may come from teaching and research institutions in France or abroad, or from public or private research centers. L'archive ouverte pluridisciplinaire **HAL**, est destinée au dépôt et à la diffusion de documents scientifiques de niveau recherche, publiés ou non, émanant des établissements d'enseignement et de recherche français ou étrangers, des laboratoires publics ou privés.

A functional operon delineates an extracellular pathway that controls body asymmetry only in animals with a ciliated left-right organizer

3

Emmanuelle SZENKER-RAVI^{1,2,\$,*}, Tim OTT^{3,\$}, Muznah KHATOO^{1,2}, Anne MOREAU DE BELLAING⁴, 4 Wei Xuan GOH¹, Yan Ling CHONG^{5,30}, Anja BECKERS^{6,7}, Darshini KANNESAN¹, Guillaume 5 LOUVEL⁸, Privanka ANUJAN^{5,31}, Vydianathan RAVI⁵, Carine BONNARD¹, Sébastien MOUTTON⁹, 6 Patric SCHOEN¹⁰, Mélanie FRADIN¹¹, Estelle COLIN¹², André MEGARBANE^{13,14}, Linda DAOU¹⁵, 7 Ghassan CHEHAB¹⁶, Sylvie DI FILIPPO¹⁷, Caroline ROORYCK-THAMBO¹⁸, Jean-François 8 DELEUZE¹⁹, Anne BOLAND¹⁹, Nicolas ARRIBARD²⁰, Rukiye EKER²¹, Sumanty TOHARI⁵, Alvin Yu 9 Jin NG⁵, Marlène RIO²², Chun Teck LIM²³, Birgit EISENHABER²³, Frank EISENHABER²³, Byrappa 10 VENKATESH^{5,24}, Jeanne AMIEL^{22,25}, Hugues ROEST CROLLIUS⁸, Christopher T. GORDON²⁵, Achim 11 GOSSLER^{6,7}, Sudipto ROY^{5,26}, Tania ATTIE-BITACH^{22,27}, Martin BLUM^{3,*}, Patrice BOUVAGNET^{28,*} 12 and Bruno REVERSADE^{1,2,5,24,29,*} 13

14

15 1. Institute of Medical Biology (IMB), A*STAR, Singapore

16 2. Genome Institute of Singapore (GIS), A*STAR, Singapore

17 3. University of Hohenheim, Garbenstr. 30, 70599 Stuttgart, Germany

18 4. Laboratoire de Cardiogénétique, Groupe Hospitalier Est, Hospices Civils de Lyon, Lyon, France

- 19 5. Institute of Molecular and Cell Biology (IMCB), A*STAR, Singapore
- 20 6. Institute for Molecular Biology, OE5250, Hannover Medical School, Carl-Neuberg-Str. 1, 30625 Hannover,

21 Germany

22 7. REBIRTH Cluster of Excellence, Hannover, Germany

23 8. Institut de Biologie de l'Ecole Normale Supérieure (IBENS), Ecole Normale Supérieure, CNRS, INSERM, PSL

- 24 Research University, 75005, Paris, France
- 25 9. Service de Génétique, CHU Dijon, 14, rue Paul Gaffarel, 21079, Dijon, France
- 26 10. Praxis Dr Patric SCHÖN, Feierabendstrasse 53, 85764 OBERSCHLEISSHEIM, Germany
- 27 11. Service de Génétique Médicale, Hôpital Sud, CHU de Rennes, 35203, Rennes cedex, France
- 28 12. Service de Génétique, CHU Angers, 4, rue Larrey, 499933 Angers, France
- 29 13. CEMEDIPP-Centre Médico-Psychopédagogique, Beirut, Lebanon
- 30 14. Institut Jérôme LEJEUNE, Paris, France
- 31 15. Unité de Cardiologie Pédiatrique, Hôtel Dieu de France, Boulevard Alfred Naccache, Achrafieh, Beirut,
 32 Lebanon
- 33 16. Department of Pediatrics, Lebanese University, Faculty of Medical Sciences, Hadath, Greater Beirut, Lebanon
- 34 17. Service de Cardiologie Pédiatrique, Groupe Hospitalier Est, Hospices Civils de Lyon, 69677 Bron, France
- 35 18. Service de Génétique, CHU de Bordeaux, place Amélie Rabba-Léon, 33076, Bordeaux cedex, France
- 36 19. Centre National de Génotypage, Institut de Génomique, Commissariat à l'Energie Atomique et aux Energies
- 37 Alternatives (CEA), Evry, France
- 38 20. Service de Cardiologie Pédiatrique, Hôpital Universitaire des Enfants Reine Fabiola (HUDERF), Brussels,39 Belgium
- 40 21. Pediatric Cardiology Division, Pediatrics Department, Istanbul Medical Faculty, Istanbul University, 34093

41 Istanbul, Turkey

- 42 22. Fédération de Génétique, Hôpital Necker-Enfants Malades, Assistance Publique Hôpitaux de Paris, 75015
- 43 Paris, France
- 44 23. Bioinformatics Institute (BII), A*STAR, Singapore
- 45 24. Department of Paediatrics, National University of Singapore (NUS), Singapore
- 46 25. Université de Paris, Imagine Institute, Laboratory of Embryology and Genetics of Malformations, INSERM
- 47 UMR 1163, 75015 Paris, France
- 48 26. Department of Biological Sciences, National University of Singapore (NUS), Singapore
- 49 27. Université de Paris, Imagine Institute, Laboratory of Genetics and development of the cerebral cortex,
- 50 INSERM UMR 1163, 75015 Paris, France
- 51 28. CPDPN, Hôpital MFME, CHU de Martinique, BP632, 97200 Fort de France, France
- 52 29. Medical Genetics Department, Koç University School of Medicine (KUSOM), Istanbul, Turkey
- 53 30. Present address: Department of Pathology, National University Hospital, Singapore
- 54 31. Present address: Institute of Reproductive and Developmental Biology, Hammersmith Hospital, Imperial
- 55 College, London, UK
- 56
- 57 \$ These authors contributed equally to this work

58

59 * Authors to whom correspondence should be addressed:

- 61 Emmanuelle Szenker-Ravi (emmanuelle.szenker@reversade.com)
- 62 Martin Blum (martin.blum@uni-hohenheim.de)
- 63 Patrice Bouvagnet (<u>patrice.bouvagnet@chu-martinique.fr</u>)
- 64 Bruno Reversade (bruno@reversade.com)
- 65
- 66

67 Abstract

68 In deuterostomes, the left-right (LR) axis is specified during embryogenesis by a transient 69 organ known as the left-right organizer (LRO). Most vertebrate animals including fish, 70 amphibians, rodents and humans deploy motile cilia in the LRO to break bilateral symmetry 71 thanks to a cilia-driven leftward flow in the extracellular space. Other vertebrates such as 72 reptiles, birds, even-toed mammals and cetaceans have non-ciliated LROs and employ 73 alternative mechanisms for LR patterning. In an attempt to identify genes whose loss during 74 vertebrate evolution follows a similar pattern, we delineated a list of five extracellular 75 proteins, of which two were hitherto unknown. We focused on a novel metalloproteinase, 76 herein named TOUT-DE-TRAVERS (TDT), which is specifically expressed in ciliated LROs. 77 Using CRISPR/Cas9 genome-editing in zebrafish and Xenopus, we demonstrate that TDT is 78 solely required on the left side of the LRO to control organ laterality. Together with MMP21, 79 another protease, TDT constitutes part of a proteolytic cascade that is downstream of 80 leftward flow but upstream of DAND5, the first asymmetrically expressed gene. This pathway 81 is clinically relevant, as we report 21 human patients with loss-of-function TDT mutations 82 presenting with recessive situs anomalies with congenital heart defects. Our findings posit 83 the existence of a functional operon that is instrumental for distinguishing left from right 84 specifically in species that rely on motile cilia in the LRO.

85

86

88 Introduction

89 The three embryonic axes of vertebrate embryos are established around gastrulation. This 90 involves the transduction of conserved signalling pathways initiated by extracellular ligands: 91 the Anterior-Posterior (AP) axis is mediated by the canonical WNT pathway, the Dorsal-92 Ventral (DV) axis is driven by the BMP pathway, while the Left-Right (LR) axis is under the control of the NODAL signaling cascade¹⁻⁷. Bilateral symmetry is broken by the directional 93 94 right-to-left flow of extracellular fluids across the ciliated epithelium of the LRO, resulting in 95 the asymmetric expression of conserved genes in the LRO and in the lateral plate mesoderm 96 (LPM).

97 The current model of flow-dependent symmetry breaking at the ciliated vertebrate LRO 98 involves several well-defined steps, which have been experimentally and genetically defined in the various model organisms, particularly zebrafish, Xenopus and mouse⁷⁻⁹. Following 99 100 canonical WNT-dependent specification of the LRO precursor tissue in superficial organizer 101 cells during gastrulation, which is marked by Foxj1, the LRO forms as a single-layer 102 epithelium in the dorsal midline of the archenteron (amphibians) or remnants thereof 103 (Kupffer's vesicle in zebrafish and ventral node in mouse). Cilia on central LRO cells become 104 motile and polarize to the posterior pole of cells in a Wnt/PCP-dependent manner. In 105 Xenopus and mouse, the LRO in fact constitutes the widened posterior part of the 106 notochordal plate, which at this stage is exposed to the archenteron lumen and flanked by 107 endodermal cells. Lateral LRO cells harbor immotile and non-polarized cilia which express 108 both NODAL/GDF1 as well as the NODAL inhibitor DAND5. A right-to-left flow of 109 extracellular fluids in the immediate vicinity of the apical cell surface of central LRO cells sets 110 in during early neurula stages. This leftward flow is then sensed by immotile cilia on lateral 111 LRO cells in a poorly defined process that involves the ion channel PKD2, which forms a 112 complex with PKD1L1. As a consequence of flow-sensing, Dand5 mRNA gets reduced 113 specifically on the left side, relieving the repression of NODAL, which signals and transfers to 114 the left LPM. There, NODAL induces the transcription of the so-called NODAL cascade

genes, NODAL itself, its feedback inhibitor Lefty as well as the homeobox transcription factor 115 Pitx2. Together, these genes determine proper asymmetric organ morphogenesis and 116 117 placement. This evolutionary-conserved program ultimately orchestrates the correct 118 positioning of the heart and other visceral organs such as the lungs, spleen and stomach i.e., situs solitus¹⁰. Defects in these processes cause heterotaxy, the abnormal formation and 119 120 arrangement of organs across the left-right axis, that can range from complete inversion of 121 symmetry (situs inversus totalis) to the selective misarrangement of organs (situs ambiguus). Heterotaxy is often associated with complex congenital heart defects (CHDs)¹¹. Laterality 122 123 defects have an estimated prevalence of 1.1/10 000 live births in humans¹² and account for approximately 3% of all CHDs¹¹. Situs inversus totalis can also occur in the context of 124 syndromic ciliopathies such as the primary ciliary dyskinesia syndrome, a sinopulmonary 125 disease (PCD; MIM244400) caused by mutations in structural components of motile cilia^{13,14}. 126

127 Genes implicated in heterotaxy (HTX) in humans include components of the NODAL pathway such as the ligands themselves, namely NODAL (HTX5; MIM601265)¹⁵ and GDF1 128 (CHTD6; MIM613854)¹⁶, their cognate cell surface receptor ACVR2B (HTX4, MIM602730)¹⁷ 129 and co-receptor CFC1 (HTX2, MIM605194)¹⁸, and the dedicated extracellular modulators 130 LEFTY2¹⁹ and DAND5²⁰. Other factors not directly related to the NODAL pathway have also 131 been reported to be mutated in Mendelian forms of heterotaxy²¹. These include structural 132 components of the motile cilia including CCDC11 (HTX6; MIM614779)^{22,23}, signaling 133 134 components that function on immotile cilia that sense motile cilia-induced fluid flow such as PKD2 (PKD2: MIM613095) and PKD1L1 (HTX8: MIM616749)²⁴, as well as downstream 135 effectors including the transcription factor ZIC3 (HTX1; MIM306955)²⁵. More recently, 136 recessive mutations in the gene coding for the Matrix MetalloProtease 21 (MMP21) have 137 also been reported to cause heterotaxy (HTX7; MIM616749)²⁶⁻²⁸, but how this 138 139 metalloprotease fits into the NODAL pathway has remained enigmatic.

140 In this study, we identify a group of genes encoding extracellular proteins that directly 141 contribute to establishing the LR axis in animal species that have kept cilia in LROs. Through

142 phylogenetic analyses, we uncovered a hitherto uncharacterized metalloprotease, which we named TOUT-DE-TRAVERS (TDT, from the French expression meaning "all upside down"). 143 144 Like MMP21, and three other genes namely PKD1L1, DAND5 and ALENDROIT (ALED, 145 a.k.a. C1orf127), we find that TDT is specifically and solely expressed in the LRO in zebrafish, Xenopus and mice. Genetic inactivation of Tdt results in fully penetrant situs 146 anomalies, downstream of leftward flow, but upstream of DAND5-mediated control of 147 NODAL propagation to the left LPM. Through rescue, epistasis and biochemical 148 149 experiments, we propose that TDT, MMP21, ALED, PKD1L1, and DAND5 form a module 150 with interdependent function in LR axis specification. Because their requirements are interlocked and strictly limited to this early developmental process, this "functional" operon 151 152 has twice been lost during evolution of the vertebrates, first in the ancestor of sauropsids 153 (birds/reptiles) and then once again in even-toed mammals and cetaceans (cetartiodactyla).

155 Results

156 At least 5 extracellular proteins have been lost in species without a ciliated LRO

157 *MMP21* has been shown to have a singular pattern of gene loss across vertebrate species²⁷. 158 While it is present in humans and mice, its homologues in cetartiodactyla have acquired 159 biallelic loss-of-function mutations, indicating that no selective pressure exists to maintain 160 *MMP21* in these mammalian species (**Figure S1**). C. Gordon and colleagues have proposed 161 that early vertebrates, including fish and amphibians, possessed MMP21, but that the gene had been specifically lost in all bird and reptile species (Figure S1)²⁷. This peculiar and 162 163 repeated *MMP21* gene disappearance/inactivation across diverse phyla appears to coincide 164 with the loss of motile cilia in central cells of the LRO in animals that utilize asymmetric cell 165 movement rather than cilia-driven flow to impart LR polarity to their developing embryos $(Figure 1a.b)^{29,30}$. 166

167 Based on this initial observation, we hypothesized that MMP21 must represent, and belong 168 to, a larger group of genes which, together, constitute a pathway specifically needed for 169 motile cilia-dependent LR patterning. We thus searched for genes that, like MMP21, are 170 present in fish, frogs, primates, rodents and odd-toed ungulates but are absent or inactivated 171 in birds, reptiles and even-toed mammals (Figure 1a). In order to focus our attention on extracellular proteins, which may include possible MMP21 substrates, we restricted our 172 173 guery to protein-coding genes that are annotated to be containing a signal peptide targeted 174 for cell surface retention or secretion (Figure 1 and Figure S1). This search produced 4 175 additional genes (Figure 1b). Two of these, *PKD1L1* and *DAND5* are already known to be 176 needed for LR patterning in various model organisms, but had not been previously reported 177 to have been lost in birds, reptiles and cetartiodactyla. Two novel genes were identified, both 178 encoding secreted proteins, which we named Tout-de-Travers (TDT) meaning "all upside 179 down", and Alendroit (ALED) which means "right side out" in French. Like MMP21, TDT and 180 ALED are both present in fish, amphibians and odd-toed mammals including rodents and

humans, but are absent or mutated in birds, reptiles and cetartiodactyla (Figure 1a,b and
Figure S1).

TDT codes for a Zn²⁺-dependent metalloproteinase belonging to the M8 peptidase family of 183 184 leishmanolysin-like metzincins (a.k.a. LMLN2). As no more than 2 ESTs exist for this gene, 185 the exon-intron structure of TDT is incompletely annotated in UCSC, Ensembl or NCBI. We 186 determined that TDT in fact spans 14 exons, and consists of 4 domains: a signal peptide, a 187 zinc catalytic domain containing the consensus His-Glu-x-x-His...His (HExxH...H) active site 188 motif and a Met-turn methionine, a cysteine-rich domain and a C-terminal transmembrane 189 domain (Figure 1c and Figure S2). Transient expression of human or zebrafish Tdt in 190 HEK293T cells showed that the encoded protease is membrane-bound and does not involve 191 a GPI-anchor (Figure S3a). This is in contrast to the TDT homolog GP63 in the Leishmania promastigote, which is GPI-anchored³¹. The zebrafish TDT protein was readily secreted and 192 193 is heavily post-translationally modified by sugar moleties which can be removed by PNGase 194 F and to a lesser extent by Endo H treatment (Figure S3b). Upon DSS-crosslinking, TDT 195 assembled into a high-molecular weight oligomer consistent with a discrete quaternary 196 structure in solution (Figure S3c).

197 ALED, currently annotated as C1orf127, encodes a protein with a signal peptide, a DUF4556 198 domain, and a C-terminal proline-rich domain. A rewarding validation of the legitimacy of our 199 evo-devo screen is the report that an ENU-induced splice mutant c.26+1G>A in the mouse 200 homologue of ALED (NM 001085505, Gm572) displays heterotaxy when bred to 201 homozygosity (MGI Direct Data Submission, ID:175213). Moreover, a single case of 202 heterotaxy in humans has recently been associated with a homozygous p.Arg113* nonsense ALED mutation³². These results encouraged us to focus our attention on *TDT*, given that no 203 204 publication has ever mentioned its existence, let alone a possible role in LR specification.

205 Tdt is specifically expressed in the LRO in zebrafish, Xenopus and mouse embryos

We hypothesized that if *TDT* is to play a role during LR patterning, its developmental expression should coincide with the formation and function of the LR organizer. Using whole 208 mount *in situ* hybridization, we examined its spatio-temporal expression in three distinct 209 vertebrate species that possess a ciliated LRO.

210 In zebrafish, tdt was found to be specifically and solely expressed from 70% epiboly to the 3-211 somite stage in dorsal forerunner cells (DFCs), which coalesce to form the Kupffer's vesicle 212 (KV), the zebrafish LRO (Figure 2a and Figure S4a). By double fluorescent in situ hybridization, tdt mRNA was confirmed to colocalize with that of the DFC marker $sox17^{33}$ 213 214 (Figure 2b). Tdt expression in the DFCs was found to be regulated by Foxi1a, a master regulator of the motile ciliogenetic program^{34,35}. Indeed, *foxj1a* depletion by morpholino 215 216 oligomer injections³⁴ completely abolished *tdt* expression in the DFCs (**Figure 2c**), although ubiquitous foxi1a overexpression using a heat shock-inducible transgenic hs::foxi1a line³⁶. 217 218 did not result in ectopic *tdt* expression (**Figure 2c**). This reveals that *foxj1a* is essential, but is 219 not sufficient, to control endogenous *tdt* expression in zebrafish DFCs and KV precursors. 220 We next assessed whether Xenopus laevis, an amphibian species which also possesses a 221 homologous tdt gene, would similarly express it during gastrulation. In situ hybridization 222 revealed a restricted expression pattern initiated after the mid-blastula transition at the 223 commencement of zygotic transcription. Tdt was first expressed at stage 10.5 in the 224 involuting marginal zone (IMZ) along a dorsal-high ventral-low gradient (Figure 2d). Dorsal 225 IMZ cells include the LRO precursors, which are internalized during gastrulation with the 226 endo- and mesodermal cell mass. Early neurulae (stage 14) showed strong tdt expression in 227 cells of the circumblastoporal collar (CBC), a structure through which involuting cells pass as 228 they enter the LRO (Figure 2d). Cellular transition from the CBC into the LRO is 229 accompanied by a dampened *tdt* signal. This spatiotemporal expression is analogous to what 230 is observed in zebrafish, and the expression in the *Xenopus* CBC closely resembles that of 231 *bicc1* which is known to be involved in LR patterning in *Xenopus* embryos³⁷.

Lastly, we performed an *in situ* hybridization in an odd-toed mammalian species, *Mus musculus,* which based on our evo-devo analysis should also display LRO-specific *Tdt* expression. The analysis of mouse embryos across gastrulation/early neurulation stages revealed strong *Tdt* mRNA levels in the ventral node from the early bud to the 4-somite stage

236 (Figure 2e). Endogenous Tdt expression was enriched in the peri-nodal crown cells and 237 became asymmetric at the 3-somite stage, suggesting a downregulation in the prospective 238 left side in response to leftward flow (Figure 2e). Notably, Tdt expression was entirely 239 abolished in mutant embryos lacking Noto, a transcription factor required for proper LRO formation upstream of FOXJ1³⁸ (Figure 2f). Altogether, these expression analyses in three 240 distinct animal models with functional ciliated LROs revealed that Tdt was specifically 241 242 transcribed under the control of the transcription factors FOXJ1 and NOTO. This singular 243 spatio-temporal regulation is consistent with TDT playing a role in the process of left-right 244 patterning during embryonic development of these species. Reptiles, birds or even-toed 245 mammals could not be examined for expression of *Tdt* homologues as these species have 246 either lost the gene altogether or have accumulated deleterious mutations, suggestive of an 247 ongoing process of gene deactivation (Figure 1 and Figure S1).

248 Knockout of tdt in zebrafish and Xenopus results in organ laterality defects

249 A partial sequence of zebrafish tdt can be found in the EST XM 002662823, but it lacks a 250 proper signal peptide sequence. We noted the presence of a possible upstream start codon, 251 which would lead to the transcription of a full-length mRNA with an additional 168 nucleotides 252 (Figure S4b, light gray). We used CRISPR/Cas9-mediated gene editing to induce frameshift 253 mutations, upstream of the catalytic domain of Tdt in order to generate knockout zebrafish 254 lines (Figure S4b). Five germline alleles with distinct frameshift mutations all leading to early 255 stop codons were obtained, outcrossed and bred to homozygosity. Despite the absence of 256 measurable nonsense-mediated decay (NMD) of the mutant tdt transcripts (Figure S4c), all 257 homozygous tdt knockout (KO) fish presented with a classical phenotype of heterotaxy (**Figure 3a-c**). Zygotic (Z) null tdt^{-} fish were fertile, allowing us to generate 100% maternal 258 zygotic (MZ) *tdt^{/-}* fish which had normal viability. The developing heart is one of the first 259 260 organs to undergo asymmetric LR morphogenesis. While control embryos showed a heart 261 tube looping to the right (D-looping) at 48 hpf, Z and MZ $tdt^{-/2}$ embryos showed cardiac 262 looping randomization by visual inspection or using the Tq(my|7:eGFP) transgenic reporter

which marks cardiomyocytes³⁹ (Figure 3a). To confirm that these laterality defects seen in 263 half of *tdf*^{/-} embryos were not the consequence of Cas9 off-target effects, we performed 264 265 rescue experiments. The injection of 250 pg of wildtype *tdt* mRNA from human or zebrafish 266 did not induce any notable phenotype in control embryos (Figure S5a-c and data not shown), but was sufficient to rescue the percentage of normal cardiac looping in 87% in MZ 267 tdt^{/-} embrvos (Figure 3a). Interestingly, injection of a catalytic-dead (CD) tdt mRNA, 268 269 harboring three missense mutations in its catalytic site (HExxH→AAxxA, p.His247Ala, 270 p.Glu248Ala and p.His251Ala) was unable to rescue the heart looping defects in larvae bereft of tdt (Figure 3a). These results demonstrate the specificity of the observed 271 phenotype, highlight the importance of the Zn²⁺-binding site for the catalytic activity of Tdt, 272 273 and suggest that generalized overexpression of *tdt* is not sufficient to cause LR anomalies. 274 Triple *in situ* hybridization allowed us to better assess the LR asymmetry defects in embryos 275 lacking tdt. Brain asymmetry is observed by expression of the leftover (lov) gene in the left 276 habenulae, the leftward heart looping can be scored by myl7 expression, while the correct positioning of the pancreas to the right side is marked by *insulin (ins)* expression (Figure 3b). 277 Only 25% of MZ *tdt*^{-/-} embryos show a normal positioning of these three organs (*situs solitus*), 278 279 while more than half displayed defects in the position of at least one organ (situs ambiguus). 280 The remaining 25% presented with a complete reversal of organ positioning (*situs inversus*) 281 (Figure 3b). Interestingly, no other ciliopathy-related phenotypes such as body curvature, kidney cysts or hydrocephalus were observed in tdt^{-} mutant embryos at 72 hpf (Figure 3c), 282 283 or in the MZ null adults that are fully viable and fertile. These results are consistent with the 284 exclusive expression of tdt in the KV, suggesting a highly specialized function of Tdt during a 285 narrow window of time for LR asymmetry establishment in this species.

We next sought to confirm the role of Tdt for LR patterning in *Xenopus* embryos. Bilateral coinjection of *tdt* CRISPR gRNA with Cas9 protein (**Figure S4d**) resulted in crispants presenting with *situs* defects, as assessed by heart and intestine looping as well as the

289 position of the gallbladder (Figure 3d). Owing to holoblastic development, this amphibian species permits the assignment of gene activity requirements in left versus right lineages^{40,41}. 290 291 To determine whether Tdt is specifically required on the left or on the right side of the LRO, 292 we generated *tdt* crispants by injecting either the left or right blastomeres at the 4-cell stage. 293 Injections on the left side of the embryos resulted in similar penetrance of laterality defects, 294 while no phenotypes were observed when tdt was inactivated specifically on the right side 295 (Figure 3d). These lineage-restricted gene inactivations demonstrated that Tdt requirement 296 for proper LR asymmetry patterning is restricted to the left side of the embryo. Similar to 297 zebrafish mutants, Xenopus crispants did not present with any additional phenotype (Figure 298 **3e**), revealing the specificity of Tdt in the control of laterality. Altogether, these knockout 299 studies performed in zebrafish and Xenopus firmly establish the role of Tdt for proper LR 300 polarity in these two vertebrate species that possess cilia in their LRO.

301 Downregulation of dand5 rescues Nodal signaling defects in tdt mutant embryos

302 To get a better understanding of the situs anomalies observed in zebrafish embryos lacking 303 tdt, earlier molecular markers of LR asymmetry were inspected. The heart looping defects 304 documented using myl7 in situ hybridization at 48 hpf could be traced back to heart jogging 305 irregularities already observable by 30 hpf (Figure 4a). The expression of the nodal-related 306 gene southpaw (spaw) and its downstream targets lefty1 and lefty2, whose asymmetric expression and involvement in vertebrate LR patterning are evolutionary conserved⁴², can 307 308 serve as early readouts for future organ laterality. In control embryos, spaw expression is 309 initiated in the posterior side and remains expressed in the left LPM at the 22-somite stage 310 (Figure 4b). Interestingly, bilateral, absent or posterior-restricted expression of spaw was observed in MZ tdt^{/-} mutants, suggestive of defective asymmetric nodal signaling (Figure 311 312 4b). The integrity of the dorsal midline, which serves as a barrier to prevent diffusion of asymmetric signals between the left and right sides⁴², was intact as judged by uninterrupted 313 314 tbxta expression at the midline (Figure S5d). Expression of the Nodal target gene lefty1 in 315 the left diencephalon was completely abolished in the absence of Tdt (Figure 4c). Similarly,

the expression of *lefty2* in the left heart primordium was largely lost in *tdt* mutants (**Figure 4d**). The inability of *spaw* expression to propagate to the anterior left part of the embryos was likely the cause for defective *lefty1* and *lefty2* expression, which in turn might account for the observed randomization of brain asymmetry and heart looping, respectively.

Similar analyses were conducted in *Xenopus tdt* crispants. Early LR asymmetry defects could be documented using *in situ* hybridization for *pitx2*, a homeobox protein that acts downstream of Nodal and Lefty to induce situs-specific morphogenesis on the left side of the embryo⁴³⁻⁴⁶. While *pitx2* was restricted to the left in control embryos, it was mostly lost or misexpressed on the right side of *tdt* crispants (**Figure 4e**). This confirms that Tdt is important for proper Nodal signaling, a view which was further supported by the observation that the expression of *nodal1* in the left LPM was lost in *tdt* crispants (**Figure 4f**).

327 We next assessed whether Tdt acts downstream or upstream of Dand5, a key secreted 328 Nodal inhibitor which is downregulated on the left of wildtype embryos in response to the leftward flow^{47,48}. The MO-mediated knockdown of *dand5* on the right side of control embryos 329 330 effectively triggered bilateral pitx2 expression and situs anomalies, consistent with the key 331 role of DAND5 in NODAL induction (Figure 4e), while left-sided MO-injections had no effect, as described previously⁴⁷. However, depletion of *dand5* on the left side of *tdt* crispants, i.e. 332 333 on the side in which Tdt is required, was sufficient to rescue the asymmetry defects observed 334 in tdt crispants (Figure 4e). This important result illustrates that derepressing Nodal 335 signalling by depleting endogenous Dand5 is able to compensate for the loss of Tdt activity. 336 Altogether, these data reveal that Tdt likely functions upstream of Dand5, where its role is to 337 enhance Nodal signalling for LR asymmetry establishment in vertebrate embryos that 338 possess a ciliated LRO.

339 Tdt is required for asymmetric dand5 expression but not for ciliogenesis

In order to more precisely delineate how TDT acts vis-a-vis endogenous Nodal signaling, we carefully recorded *dand5* expression in 8-somite stage zebrafish embryos. Compared to controls, *dand5* expression in MZ $tdt^{/-}$ zebrafish was not repressed on the left side (**Figure** 343 5a). This apparent altered response to KV fluid flow could either be the result of defective KV 344 formation, improper ciliogenesis, erratic cilia-driven flow, or poor sensing of flow on the left 345 side. Using immunofluorescence for acetylated alpha-tubulin and gamma-tubulin, we found 346 that MZ *tdf*^{/-} embryos presented with a normal-sized KV containing motile cilia with normal beating patterns (Movies S1 and S2). Cilia length and numbers did not significantly differ 347 348 from that of control embryos (Figure 5b). This suggests that ciliogenesis per se and fluid flow 349 in the LRO are not appreciably affected by the absence of Tdt, as verified by the normal 350 pattern of movement of endogenous particles that remain suspended in KV fluid (Movies S3 351 and S4). Furthermore, we found that tdt inactivation had no obvious consequence on DFC 352 migration, compaction and KV formation as revealed by sox17 staining (Figure 2a-b and 353 Figure S5e). Likewise, Tdt was not required for foxi1a expression in the DFCs or KV (Figure 354 S5f).

355 A more granular analysis in Xenopus tdt crispants revealed that the expression domains of 356 the lateral LRO markers *nodal1* and *dand5* were significantly smaller in the absence of Tdt 357 (Figure 5c,d). The asymmetric expression of dand5, which is normally repressed on the left 358 side in response to Nodal signaling, was not recorded when embryos lacked functional Tdt 359 (Figure 5d). Careful analyses of various LRO parameters such as cell surface areas, cilia 360 length and polarization as well as flow velocity and directionality (following fluorescent bead 361 application to LRO explants) revealed that no single parameter was statistically different 362 between control and *tdt* crispants (Figure 5e,f and Movie S5). These results argue that Tdt, 363 like in zebrafish, is also dispensable for ciliogenesis and cilia-driven flow in the LRO of 364 Xenopus embryos. Altogether, these analyses in zebrafish and Xenopus place Tdt as a key 365 regulator of LR development downstream of leftward flow but upstream of dand5 repression.

366 Tdt acts upstream of Mmp21

To begin to analyze the relationship between MMP21 and TDT, we propagated and characterized several *mmp21* KO zebrafish lines (**Figure S6a**). As previously reported, 50% of zygotic and MZ null *mmp21* fish displayed randomization of their LR axis^{26,27}. To test

370 whether these two genes work in parallel or epistatic pathways, we generated double heterozygous $tdt^{+/-};mmp21^{+/-}, tdt^{-/-};mmp21^{+/-}, tdt^{+/-};mmp21^{-/-}$ and double KO $tdt^{-/-};mmp21^{-/-}$ fish. 371 372 Double heterozygous fish did not show any LR defects, and no discernible increase or 373 decrease in penetrance or severity of heterotaxy was observed in double KO compared to 374 the simple KO of tdt or mmp21 alone (Figure 6a). This result suggests that when one of 375 these two genes is mutated, the absence of the other may become irrelevant, and lends 376 support to the notion that the two proteins might function in the same pathway rather than in parallel ones. Importantly, overexpression of *tdt* mRNA that was used to rescue *tdt*^{/-} mutant 377 378 fish could not rescue the situs defects of mmp21 mutants (Figure 6b), suggesting that 379 Mmp21 most likely functions downstream of Tdt since it is required for overexpressed Tdt to 380 be biologically active.

381 A careful analysis of the temporal transcription of these two proteases during zebrafish 382 development revealed that they are sequentially turned on in the LRO, with tdt expression 383 preceding that of *mmp21*, which persists several hours after *tdt* is silenced (**Figure 6c**). 384 Using in situ hybridization and RT-qPCR, we found that the endogenous expression of 385 mmp21 was significantly increased in tdt KO fish (Figure 6d,e and Figure S6b), while the 386 reverse was not true (data not shown). This phenomenon was independently confirmed in double KO *tdf^{/-}:mmp21^{-/-}* zebrafish where the NMD of *mmp21* mutant transcripts normally 387 388 observed in single *mmp21* KO embryos was overcome by transcriptional upregulation when 389 Tdt function was also absent (Figure 6e). All of these data suggest that a one-way 390 transcriptional feedback operates between Tdt and Mmp21, and that they might be part of a 391 linear epistatic pathway controlling LR specification. Taken together, our data suggest a 392 working model for the action of TDT in LR axis formation (Figure 6f). TDT works in concert 393 with at least 4 partner proteins DAND5, PKD1L1, ALED and MMP21 to form an extracellular 394 module needed to sense and propagate the NODAL/GDF1 signalling cascade. This 395 functional operon has been twice lost in vertebrates that have forgone the use of beating and 396 sensing cilia in the LRO to distinguish left from right. In the ciliated LRO, TDT acts 397 downstream of the flow which is sensed by PKD1L1. TDT is required on the left side to

ensure that *DAND5* expression is inhibited for asymmetric NODAL signalling to be
propagated to the left lateral plate mesoderm. Together with MMP21 which acts after TDT,
these two proteases form a proteolytic cascade downstream of the cilia-driven flow to
prevent *situs* anomalies in fish, frogs and humans.

402

403

3 **TDT is often mutated in patients with recessive heterotaxy**

404 As TDT is required for proper left-right asymmetry patterning in zebrafish, Xenopus and 405 presumably mice, we hypothesized that loss-of-function mutations in TDT could exist and 406 account for cases of heterotaxy in humans. To test this, we screened for germline TDT 407 mutations using targeted sequencing in a cohort of 186 index cases with congenital heart 408 defects (CHDs) (Table S1). These patients either presented with heterotaxy (extra-cardiac 409 and/or cardiac laterality defects such as dextrocardia, n=108), or without heterotaxy 410 (including isolated tetralogy of Fallot or atrial septal defect (ASD), n=78). In this cohort, we 411 identified germline homozygous TDT variations in 7 cases of CHD associated with 412 heterotaxy from 7 different families (Families 1-7) (Figure 7, Table 1 and Figure S7). We 413 then identified TDT mutations by whole-exome sequencing or targeted sequencing in five 414 additional families segregating heterotaxy (Families 8-12) (Figure 7, Table 1 and Figure 415 S7). All germline variations, homozygous patients from 11 families and compound heterozygous in family 12, were confirmed by Sanger sequencing in available family 416 417 members, and found to fully segregate with the disease according to an autosomal recessive 418 mode of inheritance (Figure 7a and Table 1). With these twelve families of distinct 419 geographical origin, we report an allelic series of 9 TDT germline mutations in 21 patients 420 with congenital heterotaxy (Figure 7 and Table 1). Among the nine germline variants 421 identified, five were missense variants affecting highly conserved residues. Three of those, 422 p.Cys296Ser (Family 8), p.Ser329Leu (Family 1) and p.Arg334lle (Families 4 and 7) are 423 within the catalytic domain of TDT which could affect the enzymatic activity of the protease.

The two others missense variants p.Ser31Phe (Families 2, 5, 11 and 12) and p.Leu414Pro 424 425 (Family 6), as well as the deletion of a single conserved residue p.Phe401del (Family 9) are 426 situated in other domains which may affect the half-life or quaternary structure of TDT 427 (Figure 7c,d and Table 1). The three last variants are classical knockout alleles including 428 two nonsense mutations p.Arg194* (Family 12) and p.Trp291* (Family 3) and a frameshift 429 mutation p.Gly382Aspfs*8 (Family 10) leading to early stop codons, which we suspect will trigger NMD of mutant TDT transcripts (Figure 7c,d and Table 1). Of the 21 cases 430 431 presenting with congenital heterotaxy, 8 had situs solitus with or without isolated 432 dextrocardia, 5 had situs ambiguus, 8 had situs inversus totalis, and nearly all had congenital 433 heart defects (CHD). As is the case for mutant *tdt* fish and frogs, there is no other ciliopathy-434 related phenotype arguing that TDT plays no other function beyond early LR specification 435 (Figure 7 and Table 1). We also note that all homozygous carriers of *TDT* mutations were 436 affected, suggesting a 100% penetrance, which is in contrast to the 25% of normal embryos 437 observed in *tdt* mutant fish and frogs. We suspect that humans will be found to have situs 438 solitus despite being mutated in TDT. This cohort of patients with heterotaxy curated by P. Bouvagnet had also been consulted to gauge how frequently *MMP21* is mutated²⁷. Hence, 439 440 we can estimate that TDT mutations account for up to 6.5% of CHD human patients with 441 non-syndromic heterotaxy which is comparable to the 5.9% that was calculated for MMP21²⁷. 442 This clinical study lends strong support to the notion that biallelic loss of TDT in Homo 443 sapiens, like in Danio rerio and Xenopus laevis, is a significant contributor for severe birth 444 defects associated with heterotaxy. Taken together, our results lend credence to the notion 445 that Tdt is essential for patterning the LR axis in these three vertebrate species that utilize 446 motile cilia in the LRO.

447 Discussion

In this study, we identify, characterize and define the clinical importance of *TDT*, a gene which was never studied before. *TDT*, which encodes a 70 kDa metalloprotease, is poorly annotated in human genome and transcriptome databases due to its very restricted spatial

451 and temporal expression pattern. In an organism's entire lifespan, TDT's transcription and 452 physiological requirement appears to be limited to a finite process which only lasts a couple 453 of hours during early embryogenesis. This unique feature has precluded obtaining sufficient 454 ESTs to properly map its exon-intron borders. As such, TDT has not been properly covered 455 by commercially-available exome platforms and has thus escaped clinical investigation, despite our data showing that it is frequently mutated in recessive forms of heterotaxy 456 457 involving CHDs. By contrast, MMP21 which has a comparable temporal expression pattern 458 and requirement for LR axis formation, is also expressed in other adult cell lineages including the skin⁴⁹⁻⁵², and its high expression has been associated with poor overall survival of 459 patients with various forms of epithelial cancers^{53,54}. To the best of our knowledge, *TDT* 460 461 stands out as the single gene in LR patterning with no other function than the one ascribed 462 here.

463 What are the substrates of TDT and MMP21?

464 Based on our phylogenetic analysis, we anticipate that the substrates of these two proteases 465 might also be important for LR specification. We cannot exclude the possibility that, while 466 being cleaved by MMP21 or TDT near the LRO, these substrates may have alternate roles 467 beyond LR specification, and thus, continue to exist in some animals that do not use cilia in 468 the LRO. Alternatively, their substrates might be part of the module that we have begun to 469 delineate this far. We note that 4 of the 5 identified genes encode proteins which have been 470 reported to be post-translationally cleaved. Beyond the necessary removal of the signal 471 peptide, TDT likely harbors a prodomain with a conserved cysteine-switch which needs to be removed for full activity⁵⁵, PKD1L1 has been shown to be cleaved within the third intracellular 472 loop of its transmembrane region⁵⁶, and DAND5, like its close homologue CERBERUS, may 473 undergo proteolytic cleavage^{57,58}. Future investigations will need to address if ALED is also 474 475 cleaved or if other proteins not yet identified in this evo-devo screen might serve as 476 substrates for MMP21 and TDT. Whatever these may be, we propose that an extracellular 477 proteolytic cascade is likely at play during LR specification. This is reminiscent of another evolutionary-conserved extracellular proteolytic cascade that imparts embryonic polarity.
Patterning of the DV axis is mediated by the controlled cleavage of Chordin by the Zinc
metalloprotease Tolloid which frees BMP to signal in ventral most regions of the embryo
when Sizzled is silenced^{59,60}.

482 Evo-devo of LR specification: a functional operon twice disappears

483 Our phylogenetic screen for genes that have disappeared in vertebrate species as a 484 consequence or cause of de-ciliation of the LRO yielded important evolutionary insights into 485 the developmental programs of LR specification. Indeed, all 5 genes: TDT, ALED, MMP21, 486 DAND5 and PKD1L1 were found by us, and others before, to be expressed in the very tissue 487 and at the correct time to play a role in LR axis formation. These genes are not physically 488 linked on the same chromosomal location, and as such escape the traditional definition of an operon⁶¹. However, they seem to be functionally interlocked in a transcriptionally coordinated 489 group⁶², which we propose might be referred to as a "functional operon" for LR patterning. 490 491 The facultative nature of this "evo-devo module" is striking, since with enough time, all of 492 these genes were lost in reptiles/birds or became pseudogenes in cetartiodactyla. Forming 493 an integrated module for flow sensing and propagation of NODAL/GDF1 signalling 494 downstream of cilia-driven flow, we suspect that like a bidirectional domino-effect, if any 495 given gene becomes inactivated, all other 4 will too become obsolete. We find that this has 496 happened not once but twice during vertebrate evolution. We suspect that this was allowed 497 to happen because NODAL-dependent LR axis formation preceded cilia and flow-dependent 498 symmetry breaking during animal evolution. Lophotrochozoans, such as snails, activate left-499 asymmetric Nodal signaling independently of cilia, but via chiral cleavage patterns. Such patterns can still be seen in amphibians such as Xenopus⁶³, but have become functionally 500 obsolete during amniote evolution^{30,64}. Upon loss of ciliated LROs, cytoskeletal asymmetries 501 502 such as the ones underlying chiral cleavage may have become functional again, for example 503 as seen in chiral cell migration at the chick Hensen's node²⁹.

504 This brings an important question as to whether birds/reptiles and even-toed 505 mammals/cetaceans have found identical ways to cope with the loss of these genes or have 506 instead deployed different strategies. If so, existing pathways that can provide buffering or 507 functional redundancy might have been mobilized in both phyla. This paradigm is of 508 immediate importance since we note that canines and felines (Figure S1a), have already 509 begun to lose ALED but still harbor what appears to be normal genes for TDT, MMP21, 510 DAND5 and PKD1L1. This indicates that an ongoing forfeiture of this functional module might 511 be occurring contemporarily. If so, this should allow to settle the corollary question as to 512 which comes first. Is it the de-ciliation of the LRO that triggers the obsolescence of this 513 functional operon, or is it the loss of one of these 5 genes that specifically turns off the program of ciliogenesis within the LRO? Observing the organizer of canine or feline embryos 514 515 might help us answer this egg/chicken dilemma and give evolutionary biologists the 516 opportunity to investigate how evo-devo traits become fixed or purged in coeval vertebrate 517 species.

518

520 Methods

521 Phylo-genomic analysis

522 We scanned the 23904 phylogenetic trees of the Ensembl (version 93) Compara database to 523 identify genes with a presence/absence pattern in extant species similar to the MMP21 524 evolutionary profile. We restricted the trees to 75 species with minimal genome assembly 525 contiguity (50% of scaffolds/chromosomes must contain at least 25 genes). To identify 526 MMP21-like patterns, we searched for evolutionary histories from the Amniote ancestor that maximize retention in Euarchontoglires and Zoomata and Iosses in Artiofabula and Sauria 527 528 using the following score: $S = P_{Eu} + P_{Zoo} - 3P_{Art} - 2P_{Sau}$. Eu, Zoo, Art and Sau represent 529 respectively Euarchontoglires (primates and rodents, 39 species), Zoomata (horse and 530 carnivores, 6 species), Artiofabula (even-toed ungulates excluding camelids, 4 species) and 531 Sauria (birds and reptiles, 5 species). P represents the proportion of species in each clade 532 that retained at least one copy of the gene in the clades noted in indices. We applied higher 533 weights on gene losses in Artiofabula and Sauria because these are the distinctive features 534 of the desired evolutionary pattern, although with less emphasis on losses in Sauria owing to 535 the greater evolutionary distance to the other groups. All genes should also possess an ortholog in actinopterygian (ray-finned) fish to be considered further. Finally, we only 536 537 considered genes with proteins containing a predicted N-terminal signal peptide using 538 SignalP version 5.0⁶⁵. Genes displaying a phylogenetic score > 1 and fulfilling these criteria 539 are MMP21, DAND5, TNFRSF14, PKD1L1, ALED (C1orf127) and TDT (LMLN2) (Table S2). 540 We considered TNFRSF14 as false positive because despite its high phylogenetic score, it is 541 present in the lizard genome. As nothing was known about TDT, we decided to focus our 542 functional analysis on this gene.

543 We then specifically analyzed the presence or absence of the *ALED*, *DAND5*, *MMP21*, 544 *PKD1L1* and *TDT* genes in various groups of animals (mammals, birds, reptiles, amphibians, 545 ray-finned fishes, cartilaginous fishes, jawless vertebrates, cephalochordates, echinoderms 546 and insects) using TBLASTN searches against their respective genome assemblies at NCBI

547 with human protein sequences as queries. The genomic region encompassing the High-548 scoring Segment Pair (HSP) was extracted and searched against the NCBI NR protein 549 database using BLASTX to confirm the identity of the gene. Each BLAST HSP was then 550 manually verified and checked for the presence of frameshifts/stop codons (if any). Synteny 551 information for each of these genes was obtained from various sources such as the UCSC 552 Genome Browser (http://genome-euro.ucsc.edu/), Genomicus browser 553 (https://www.genomicus.biologie.ens.fr/genomicus-99.01/cgi-bin/search.pl), NCBI Genome 554 Data Viewer (https://www.ncbi.nlm.nih.gov/genome/gdv/) and Ensembl genome browser 555 (http://asia.ensembl.org/index.html).

556 *Comparative genomics*

557 Comparative analysis of the TDT protein family was performed using the NCBI reference 558 sequences of the following species with modifications: human (Homo sapiens; 559 LOC100128908, BC153822, IMAGE:40134016, LMLN2-204 with addition of the conserved 560 exons 5, 11, 12, 13 and 14, Figure S2), rabbit (Oryctolagus cuniculus; LOC103351174, 561 XM_008269362.1, XP_008267584.1), gray mouse lemur (Microcebus *murinus;* 562 LOC105864643, XM 012752611.1, XP 012608065.1), ferret (Mustela putorius furo; 563 LOC101683375, XM 004755331.2, XP 004755388.1), mouse (Mus musculus; 564 LOC101056084, XM 006519864.2, XP 006519927.2), rat (Rattus norvegicus; 565 RGD1560492, XM 008770711.2, XP 008768933.1), zebrafish (Danio rerio; LOC100331300, 566 XM 002662823, XP 002662869.2 using a START Methionine located 56 amino acids 567 upstream of the predicted one, Figure S4b). We used the following coordinates for the full 568 length ORF of human TDT (chr14:23,104,920 - 23,099,282): BC153822/LMLN2-204 with 569 extra exons 5 (23,103,051-23,102,926), 10 (23,101,765-23,101,669), 11 (23,101,564-570 23,101,292), 12 (23,101,079-23,100,850), 13 (23,100,681-23,100,502) and 14 (23,099,489-23,099,282). To identify the orthologous proteins of TDT, the genome sequence databases 571 572 were searched using BLASTP and TBLASTN. The TDT protein or deduced amino acid sequences from all 7 species listed above were aligned using ClustalO⁶⁸. 573

574 Constructs

Full length human TDT (as described above) was synthesized (Genscript) and cloned into the pCS2+ vector. Zebrafish Tdt cDNA (as described above) was cloned from the XM_002662823/ODa12959 clone (Genscript) to which we added the 168 missing nucleotides using a gBlock (IDT) and cloned into the pCS2+ vector. For the zebrafish TDT- Δ TM construct, a STOP codon was introduced before the transmembrane domain. The human CD109 cDNA was also cloned into the pCS2+ vector with a N-terminal FLAG tag.

581 TDT antibodies

582 TDT Polyclonal antibodies were raised against the human epitope: 583 CWKKENGFPAGVDNPHGEI, and the zebrafish Tdt epitope: CWIEDNARSGMNEGGGEI within the cysteine-rich domain, and peptide-affinity purified from 2 rabbit sera each (GL 584 585 Biochem).

586 HEK293T cell culture and treatments

587 HEK293T (from ATCC) cells were cultured on plates coated with poly-L-lysine (Sigma P4707) with the following medium: DMEM high glucose (HyClone SH300081.01) with 10% 588 fetal bovine serum (Thermo Scientific SH30070), and 2 mM L-glutamine (ThermoFisher 589 590 Scientific 25030081). Cells were transfected with DNA plasmid using the FuGENE HD 591 transfection reagent (Promega E2312) in OptiMEM medium (Gibco 31985070). For protein 592 extraction, cells were lysed using an appropriate amount of RIPA buffer (Tris-HCl pH7.5, 50 593 mM, NaCl 150 mM, NP-40 0.1%, Na2+-deoxycholate 0.05%) supplemented with proteinase 594 inhibitors (Complete, Roche 04693159001). Lysates were centrifuged at 17,000g for 15 min 595 at 4°C to remove cell debris, and the supernatants (protein extracts) were collected. For 596 secretion studies, culture medium was changed 24 h after transfection with a serum-free 597 medium Pro293a-CDM (Lonza 12-764Q) supplemented with L-glutamine. Secretion was 598 allowed for 48 h before collection of the conditioned media. For Phosphatidylinositol-specific 599 Phospholipase C (PI-PLC) treatment, culture medium was changed 48 h after transfection

600 with serum-free medium without or with 1 U/mL of PI-PLC (Molecular Probes, P-6466), cell 601 culture plates were then placed at 4°C for 20 min rotating before cell lysate and medium 602 extraction. For EndoH (NEB #P0702S) and PNGaseF (NEB #P0704S) treatments, 603 conditioned media were treated as per the manufacturer protocols. For DSS crosslinking 604 experiments, conditioned media were first dialysed overnight in PBS at 4°C and then DMSO or 3 mM final disuccinimidyl suberate (DSS in DMSO) was added to the dialysed conditioned 605 606 media. The mixture was then incubated at room temperature (RT) for 1 h with maximum 607 shaking of 2000 rpm on a tabletop shaker. The reaction was stopped by the addition of 60 608 mM final of Tris pH 7.5 and incubated for another 30 min at RT, shaking at 2000 rpm on a 609 tabletop shaker.

610 Western blotting

611 For western blotting, samples were electrophoresed with reducing Laemeli loading buffer 612 after denaturation at 95°C for 10 min. The protein ladder (Bio-Rad 161-0377) and denatured 613 and reduced samples were loaded onto 4-20% gradient precast gels (BioRad Criterion 567-614 1093) in 1x running buffer (25 mM Tris, 200 mM glycine, 0.1% SDS) and ran at 80–180 V 615 until desired separation. Gels were transferred onto 0.2 µm PVDF membranes (BioRad 616 Criterion 170-4157) using the Trans-Blot TurboTM transfer system for 7 min. Membranes 617 were blocked for 1 h at room temperature with 5% milk in TBST (50 mM Tris-HCl pH 7.5, 150 618 mM NaCl; with 0.05% Tween20). Membranes were incubated with primary antibody diluted 619 in 5% milk in TBST at 4°C overnight (anti-Flag, 1:1,000, Cell Signaling 14793 S; anti-620 GAPDH, 1:4,000, SantaCruz 47724, anti-zfTdt, 1 µg/mL, in-house; and anti-hTDT, 1 µg/mL, 621 in-house). After washes in TBST, membranes were incubated for 1 h at room temperature 622 with secondary antibodies (Mouse-HRP 71503510 or Rabbit-HRP 711035152, 1:4,000, 623 Jackson Immuno) in 5% milk in TBST. After several washes in TBST, the signal was revealed with the HRP substrate (Thermo Scientific SuperSignal 34080/34076/34096) for 3 624 625 min at room temperature. Membranes were then exposed to CL-Xposure films (Thermo 626 Scientific 34091), and developed in a Carestream Kodak developer.

627 Mouse husbandry and lines

Mice were handled in accordance with the German laws and regulations (Tierschutzgesetz). All procedures were approved by the ethics committee of Lower Saxony for care and use of laboratory animals LAVES. Mice were housed in the animal facility of Hannover Medical School (ZTL) as approved by the responsible Veterinary Officer of the City of Hannover, Germany. Animal welfare was supervised and approved by the Institutional Animal Welfare Officer. *Noto^{-/-}* mutant mice (*Noto^{eGFP/eGFP}*) were described previously⁶⁹.

634 Mouse whole mount in situ hybridization (WISH)

635 Mouse WISH was carried out on E7.0-8.5 (late streak till 6-somite stage) old mouse embryos using standard procedures in detail described in⁷⁰. The DIG-labelled antisense RNA probes 636 637 were generated using the DIG RNA labelling system (Roche). DIG-labelled probes were 638 detected with BM-Purple AP substrate (Roche). WISH results were documented with the 639 Leica DM5000B microscope with Leica Firecam software. Mouse Tdt-probes (Gm29776; 640 ENSMUST00000224691.2) were synthesized with T7 RNA-polymerase from a linearized 641 pCRII-TOPO vector (Invitrogen) containing the following inserts: "Tdt-5' part", a 926 bp 642 fragment (exons 3-11) amplified with the forward 5'- AGATTCCAGATGCCCACCTGC-3' and 643 reverse 5'- GCAGCGACTGTGCCTATGGTA-3' primers; or the "Tdt-3' part", a 739 bp 644 fragment (exons 11-14) amplified with forward 5'-TACCATAGGCACAGTCGCTGC-3' and 645 reverse 5'-GGAGCATAGCCCGTTTCTGGT-3' primers. Template for PCRs was cDNA from 646 wildtype (CD-1 mouse) E7.5 whole embryos. The cDNA was generated from total RNA using 647 SuperScript II Reverse Transcriptase (Invitrogen) and Oligo(dT) priming.

648 Zebrafish husbandry and lines

Zebrafish (*Danio rerio*, AB line) were maintained and used according to the Singapore National Advisory Committee on Laboratory Animal Research Guidelines (Institutional Animal Care and Use Committee (IACUC #161172). Zebrafish embryos were grown at 28.5°C in egg water as previously described⁷¹. The Tg(hsp70::foxj1a) line was recently

described³⁶. For induction of the *foxi1a* transgene, a 1 hr heat shock was administered at 653 50% epiboly and embryos were fixed at the 90% epiboly stage. The tdt mutant line was 654 655 generated using CRISPR/Cas9 genome editing technology, as previously described⁷². In 656 brief, a custom gBLOCK (Integrated DNA Technologies) was designed incorporating a guide 657 RNA-targeting sequence preceded by a T7 promoter sequence. The targeted sequence on 658 the exon 4 of the tdt gene was 5'-GTCCCAACAGTGCTGAGGCC-3' with a guide RNA 659 sequence of 5'-GGCCTCAGCACTGTTGGGAC-3'. The gRNA was synthesized using the MEGA shortscript[™] Kit (Applied Biosystems), and was purified using the RNeasy Mini Kit 660 661 (QIAGEN). Cas9 mRNA was synthesized using the mMESSAGE mMACHINE® Kit (SP6) 662 from a Notl-linearized zebrafish codon-optimized Cas9 construct in pCS2+ (gift from Tom 663 Carney, Singapore). The gRNA and Cas9 mRNAs were mixed together to a concentration of 664 250 ng/µL each, and 2 nL was injected into the yolk of one-cell stage AB zebrafish embryos. 665 A 5 bp insertion allele resulting in a frameshift and premature stop codon at amino acid 171 666 was isolated (Line 1, Figure S4b). Additional alleles were isolated (Lines 2-5, Figure S4b) 667 showing an equivalent phenotype at the homozygous state (data not shown). Mmp21 668 zebrafish crispants were a gift from Nicholas Katsanis (Duke Med, USA) and were described previously²⁶. Three distinct alleles leading to a frameshift with an early stop codon were 669 670 isolated (Figure S6a), all showing an equivalent phenotype (data not shown). Here, we 671 focused on the allele with a complex 10 bp deletion leading to a frameshift at amino acid 38 672 (Line 3, Figure S6a). The heart looping (normal, inverted or no looping) was scored at 48 673 hours post fertilization (hpf) while embryos were still in their chorion.

674 Genotyping of zebrafish mutants

The *tdt* mutants could be genotyped by sequencing a 484 bp product containing exon 4 amplified with the following forward 5'-TGTTGGAAACCTGGAACCAT-3' and reverse 5'-ATGGTTCCAGGTTTCCAACA-3 primers. The *tdt* Line 1 was genotyped by allele-specific PCR with the same two primers as well as an internal forward primer annealing specifically to either the wildtype (wt): 5'-AATCCTGAGCATCCAGTCCC-3', or the mutant: 5'-

AATCCTGAGCATCCAGTCAG-3' allele, leading to an additional amplicon of 142 bp or 149 bp, respectively. The *mmp21* mutants were genotyped by sequencing a 240 bp product in exon 1 amplified with the following forward 5'-GAATAAATGCGTGTGGAGTTCA-3' and reverse 5'-ACTGCAAAATACAAAATGTGCG-3' primers.

684 Zebrafish in situ hybridization

Whole mount in situ hybridization (WISH) was carried out using DIG-labelled and fluorescein-685 labelled antisense probes as previously described⁷³. Fluorescein-labelled probes were 686 687 detected using INT/BCIP and DIG-labelled probes with NBT/BCIP. Probes were synthesized with Sp6 or T7 polymerases from a linearized pGEMT-easy vector containing the following 688 689 inserts: for tdt, a 365 bp fragment between exons 8-10 was amplified with the forward 5'-690 TGTGCTTCAGGGCTCCATTA-3' and reverse 5'-TCTCTCCGCCTCCTTCATTC-3' primers ; 691 for lov, a 631 bp fragment in the single exon was amplified with the forward 5'-692 ACCCCGAGTGTGGAATATCA-3' and reverse 5'-TCTCCAAACACCTCCTTTGC-3' primers : 693 for dand5, a 609 bp fragment in exon 2 was amplified with the forward 5'-694 GTCAGTGCAGCTCCATGTTC-3' and reverse 5'-CCAATTAATATTTCGGCCACTT-3' 695 primers; for myl7 (cmlc2), a 246 bp fragment between exons 2-5 was amplified with the 696 forward 5'-ATACAGGAGTTTAAGGAGGC-3' and reverse 5'-GTCGAACAATTTAAAAGCAG-697 3' primers ; for ins, a 437 bp fragment between exons 1-3 was amplified with the forward 5'-698 CCATATCCACCATTCCTCGC-3' and reverse 5'-CAAACGGAGAGCATTAAGGC-3' primers ; 699 lefty1, the complete cDNA amplified with the forward 5'for was 700 GCACAGCAGTGACAGCTTCT-3' and reverse 5'-TTCAGTCAGTCTCACATATA-3' primers ; 701 for lefty2, a 465 bp fragment in exon 4 was amplified with the forward 5'-702 ATCCCAAGGCAACTGTAACT-3' and reverse 5'-AAGCTTACATTACATAAAGC-3' primers ; 703 for tbxta (*ntl*), the complete cDNA was amplified with the forward 5'-CGCTGTCAAAGCAACAGTAT-3' and reverse 5'-GAACTCCTTTTTTTGACAG-3' primers ; 704 705 for sox17, a 961 bp fragment between exons 1-2 was amplified with the forward 5'-706 TGAATGAACTGTATGCACTC-3' and reverse 5'-TGCAGGTTTATTGAACTGAG-3' primers ;

and for *foxj1a*, a 634 bp fragment between exons 1-2 was amplified with the forward 5' CATCAAGCCGCCATACTCAT-3' and reverse 5'-TGAATCCAGTAGAGCGTCCC-3' primers.

709 Zebrafish mRNA and morpholino injection

710 Embryos were injected at the one-cell stage according to standard procedures. For 711 overexpression/rescue experiments, SP6-transcribed full length zebrafish tdt capped mRNA 712 (mMessage mMachine SP6 transcription kit, Thermofisher #AM1340) was injected into one-713 cell stage embryos at the indicated concentration. The catalytic dead (cd) Tdt corresponds to 714 p.His247Ala, p.Glu248Ala and p.His251Ala mutations (HExxH to AAxxA). The mmp21 splice-715 blocking morpholino oligonucleotide (MO) 5'-GTTGTATATTTGTTCACTGACCCGT-3' has 716 been described previously²⁷. The foxj1a translation-blocking MO 5'-717 CATGGAACTCATGGAGAGCATGGTC-3' was previously described³⁴.

718 Zebrafish real-time qPCR

719 For qPCR experiments, embryos at indicated stages were lysed in the QIAGEN RLT buffer 720 and total RNAs were extracted using the QIAGEN RNeasy Mini kit (74106), including the 721 optional DNase RNase-free treatment. cDNAs were obtained using the iScript reverse 722 transcription supermix (Bio-Rad 170-8841). gPCR were performed with the following primers 723 using the Power SYBR Green Master mix (Applied Biosystems 4367659) on the Applied 5'-724 Biosystems 7900HT Fast Real-Time PCR system. zf tdt-gPCR-F: 725 CGATGCTGACTTCCTGCTTT -3'; zf tdt-qPCR-R: 5'-GAACCCGTCTGACAGTGAGC -3'; 726 zf mmp21-gPCR-F: 5'-GGACCGCAAATCTATCCAGA-3' ; zf mmp21-gPCR-R: 5'-CGTCTGCTCCTTTCTGATCC-3'; zf actin-qPCR-F: 5'-GATCTTCACTCCCCTTGTTCA-3'; 727 zf actin-qPCR-R: 5'-GGCAGCGATTTCCTCATC-3'. Data are average of at least three 728 729 biological triplicates and statistical analyses were done with the PRISM5® software using a 730 one-way ANOVA test with Bonferroni correction for multiple hypothesis testing when more 731 than two groups were compared, or an unpaired t-test with Welch's correction when less than 732 three groups were compared. Non-significant (ns) indicates a p-value of p>0.05 and asterisks

indicate p-values of p<0.05(*), p<0.01(**) and p<0.001(***). Error bars indicate standard error
of the mean (s.e.m.).

735 Zebrafish immunofluorescence

Wildtvpe and *tdt^{/-}* mutant 10-somite embryos were fixed for 2 hours at room temperature in 736 737 4% paraformaldehyde (PFA) in PBS. The embryos were stored in methanol at -20°C, and 738 then rehydrated in a gradient of PBS/methanol. The embryos were permeabilized in acetone, 739 blocked in PBDT (PBS, 1% BSA, 1% DMSO and 1% Triton X-100) plus 5% sheep serum. 740 Embryos were incubated with primary and secondary antibodies and washed in PBDT. The 741 primary antibodies used were anti-acetylated-alpha-tubulin (rabbit monoclonal, Cell 742 Signaling, 5335S), anti-acetylated-tubulin (monoclonal, Sigma, T6793), anti-gamma (y)-743 tubulin (monoclonal, Sigma, T6557) and the secondary antibodies used were Alexa 744 fluorophore-labeled anti-mouse and anti-rabbit (Molecular Probes). Immunofluorescence 745 images were captured on an Olympus Fluoview 1000 microscope with 60 x, 1.4 NA oil 746 immersion objectives.

747 Zebrafish KV movies

For analysis of cilia motility in KV and movement of endogenous particles suspended in KV fluid, appropriately staged zebrafish embryos were embedded in 1.5% low-melting-point agarose on 50 mm glass-bottom dishes. Ciliary motility and particle movement were viewed with a Zeiss 63X water-dipping objective on a Zeiss Axioplan2 (upright) microscope equipped with an ORCA-Flash4.0 V2C11440-22CU camera (Hamamatsu). Processing of videos and was performed with ImageJ 1.44d (NIH, USA).

754 Xenopus husbandry and injection experiments

Handling of *Xenopus laevis* frogs (Nasco) was in accordance with the German laws
(Tierschutzgesetz), and was approved by the Regional Government Stuttgart, Germany.
Animal welfare was supervised and approved by the Institutional Animal Welfare Officer.
Embryos were injected in Ficoll medium (1x MSBH and 2 % Ficoll) at the 1- or 4-cell stage,

759 and were further cultivated in 0.1x MSBH. Xenopus laevis tdt crispants were created with a gRNA 5'-GGGGAAGTCAGGGATCTAGG-3' designed via CRISPRscan⁷⁴ targeting the splice 760 761 acceptor site of exon 4. gRNA templates harboring a T7 promoter were assembled using oligo extension reaction⁷⁵. The gRNA was transcribed using the MEGAshortscript T7 762 Transcription Kit (Invitrogen) in combination with the MEGAclear Transcription Clean-Up Kit 763 764 (Invitrogen). Ribonucleoproteins (RNPs) consisting of gRNA and Cas9 protein (PNA Bio) 765 were pre-assembled at 37°C for 5 min and in total 1 ng Cas9 protein was injected together 766 with 150 pg gRNA. Genome editing was confirmed via direct sequencing of PCR products 767 using the following forward 5'-AAAGTGTTTGGACGTCACAGT-3' and reverse 5'-TCACCTGAGCTGCACATTTCT-3' primers⁷⁵. Efficiency was determined using the Synthego 768 ICE analysis tool⁷⁶. 769

770 Xenopus in situ hybridization

771 WISH was performed using DIG-labelled antisense probes in combination with BM-Purple staining solution (Roche) as previously described⁷⁷. All probes were transcribed from 772 773 linearized plasmids using T7 or SP6 RNA polymerases (Promega). For tdt, a 774 bp 774 fragment from 1 was amplified with the 5'exon following forward 775 ACACCCACTTGTACATCGCT-3' and reverse 5'-GCAGGGCAATCTTCAGTTGT-3' primers.

776 Xenopus immunofluorescence

777 Embryos were fixed at stage 17 overnight at 4°C in 4% PFA in PBS⁻ and stored in fixative. 778 The specimens were permeabilized in PBST (PBS, 1% Triton X-1000) and blocked in CAS-779 Block (Thermo Fisher). Embryos were subsequently incubated with the primary anti-780 acetylated- α -tubulin 6-11B-1 antibody (1:700 dilution, Sigma, #T6793) followed by the 781 secondary anti-mouse IgG Cy3 antibody (1:1000 dilution, Merck) in combination with Alexa 782 Fluor 488 Phalloidin (1:200 dilution, Thermo Fisher). Imaging was performed on a Zeiss 783 Observer.Z1 microscope with a Zeiss Plan-Apochromat 20x, 0.8, objective coupled to a 784 Zeiss LSM 600.

785 Xenopus LRO movies

Leftward flow was analyzed as previously described⁷⁸. In brief, dorsal explants were crafted 786 787 at stage 17 and bathed in a solution of yellow-green fluorescent 0.5 µm FluoSpheres 788 (1:3000, 1x MSBH, Invitrogen). Explants were placed in a chamber made from duct tape, a 789 slide and a cover slip. 1 min time-lapse movies of the flow were captured on a Zeiss 790 Axioskop 2 mot plus microscope with a Zeiss Plan-Neofluar 20x, 0.5, objective in 791 combination with a Zeiss Hsm Camera at 2 FPS. Particle trajectories were traced with the ImageJ⁷⁹ plugin Particle Tracker⁸⁰. Measurements of the trajectories and the visualization of 792 793 the particle movements in gradient-time-trails (GTTs)⁷⁸ was done with a custom-made script written in R⁸¹. 794

795 Human study participants

The study included 57 individuals from 12 families, of which 21 individuals were affected with left-right asymmetry defects. Families ethnologically originated from France (Families 5, 8, 11 and 12), Turkey (Families 1, 2, 4, 6 and 7), Italy (Family 3) and Lebanon (Families 9 and 10) (**See Figure 7 and Table 1**). The study protocol was approved by A*STAR IRB (2019-087) and genetic analyses were performed in accordance with bioethics rules of French laws. Written informed consents were obtained from all the participants or parents.

802 DNA extraction, quantification, and quality control

Genomic DNA of the affected individuals and other available family members was extracted from either whole blood or fetal tissue using a variety of extraction protocols. DNA concentration and quality were assessed using NanoDrop (Thermo Scientific) and Qubit (Life technologies) fluorometers. A260/A280 ratios of 1.8 to 2.0 and A260/A230 ratios >1.5 were accepted. DNA fragmentation was assessed using agarose gel (0.8%) electrophoresis.

808 Genome-wide genotyping

For Families 1, 2, 3, 6 and 7, minimal amount of 1 microgram at a minimal concentration of

50 ng/mL of each gDNA was used for genotyping on HumanCoreExome-12 v1.0 (WG-353-

811 1104) arrays (Illumina, San Diego, USA) according to the Illumina protocol 'Infinium HD Ultra 812 Assay Automated EUC (11328108 B)' (Illumina, San Diego, USA). The arrays were scanned 813 on an IScan+ scanner. Genotyping results were obtained using GenomeStudio (Illumina, San 814 Diego, USA). Quality controls were performed on inner house controls, and control DNA. 815 Genotyping and pedigree information were compared (sex, familial relationship, mendelian allele segregation) with Linkdatagen^{82,83}, a PERL script that generates datasets for linkage 816 817 analysis, relatedness checking, IBD and HBD inference. Parental relatedness was also 818 checked with Graphical Representation of Relationships (http://csg.sph.umich.edu/abecasis/GRR/index.html)84. Linkdatagen created output files for 819 MERLIN⁸⁵. Parametric (disease allele frequency of 0.0001, a fully penetrant disease, and a 820 821 0% phenocopy rate, autosomal recessive inheritance) and non-parametric analyses were 822 performed. Haplotypes of the region of interest were prepared with GeneHunter. Genehunter 823 output files were used to visualize haplotypes with the Haplopainter 1.043 software⁸⁶. Two-824 point analyses (between the disease phenotype and TDT mutations) were carried out with EasyLinkage⁸⁷ and Superlink v1.6 (http://bioinfo.cs.technion.ac.il/superlink/) with a disease 825 826 allele frequency of 0.0001, a phenocopy rate of 0%, an autosomal recessive inheritance and 827 a penetrance value of 100%.

828 For Family 8, genome-wide linkage scans were performed using the Affymetrix SNP 10K2.1 829 array (Affymetrix, Santa Clara, CA, USA) in the two affected individuals (V:2 and V:4) and 830 their healthy sister (V:3). These data were analyzed by calculating multipoint lod scores 831 using MERLIN software and assuming a recessive inheritance with complete penetrance 832 thanks to a collaboration with Dr. Emmanuelle GENIN. The region of homozygosity on 833 chromosome 14 was confirmed and refined by haplotyping with microsatellite markers 834 selected on the UCSC browser. The microsatellite markers were amplified in a multiplex 835 manner using the QIAGEN Multiplex PCR kit. The amplification products were finally analyzed on an ABI Prism 3130 analyzer (Applied Biosystems). The haplotyping of the 836 837 markers has been optimized using Genescan Analysis and Genotyper softwares.

838 Ampliseq design, library preparation and targeted sequencing

839 Targeted sequencing was used in Families 1-7, and 11-12. In brief, the 14 exons including 840 UTRs and 20 intronic nucleotides on each side of each exon of the TDT gene, along with 2 841 other genes (total target region: 32450 nucleotides, total target on TDT: 4039 nucleotides) 842 were selected to generate primers according to Ampliseq Designer (https://www.ampliseg.com/) with a predicted TDT sequencing coverage of 100%. Pools of 6 843 844 gDNA samples were prepared by pooling together gDNA extracted with the same protocol. 845 For library construction, 5ng of pooled DNA was amplified using the customized panel 846 (Ampliseq, Thermo Fisher). The amplicons were then partially digested, barcoded and amplified using the Ion Ampliseg[™] Library kit 2.0 and Ion Xpress[™] barcode adapter kit 847 848 (Thermo Fisher) according to manufacturer instructions. The library was quantified using the 849 Qubit fluorometer and the BioAnalyzer 2100 (Agilent). Libraries were multiplexed at a final concentration of 15 pM, and 25 µL were clonally amplified on Ion sphere[™] particles (ISP) by 850 851 emulsion PCR performed on the Ion One Touch 2 instrument (Thermo Fisher) according to manufacturer instructions. Quality control was performed using the Ion Sphere[™] Quality 852 853 Control kit (Thermo Fisher) to ensure that 10-30% of templates positive ISP was generated in the emulsion PCR. Finally, the template ISP were enriched, loaded on an Ion 318[™] chip 854 v2 and sequenced on a PGM[™] sequencer with the Ion PGM[™] sequencing 200 kit v2 855 856 according to manufacturer instructions. Quality of sequencing was assessed by the PGM 857 sequencer by providing the Ion Sphere Particle (ISP) density, number of total reads, 858 percentage of usable reads, percentages of monoclonal and polyclonal reads, mean read 859 length (AQ17, AQ20 and perfect), percentages of low quality sequences, adapter dimers and 860 aligned bases. Bam files were loaded on Alamut Visual 2.5 (Interactive Biosoftware, Rouen, 861 France) and variant detection was performed manually by setting the variant detection threshold to 0.04. STOP gain, splice site, frameshift and rare missense variants (< 0.1%) 862 863 were selected for Sanger sequencing of the 6 individual DNA composing the pool carrying 864 each selected variant. Variants of interest were confirmed on a second dilution of DNA and

on an independent sample. Subsequently, relatives with available gDNA samples were
 tested for variant segregation analysis.

867 Exome sequencing

868 Exome sequencing was employed independently for the detection of variants in Family 8 869 (Trio analysis with individuals IV:1 (mother), V:2 (patient) and V:4 (affected sister)), Family 9 870 (IV:1 (patient) and IV:3 (affected brother)), and Family 10 (IV:2 (patient)). One microgram of 871 high-quality gDNA was used for exome capture with the ION TargetSeq Exome Kit. The 872 exome library was prepared on an ION OneTouch System and sequenced on an Ion Proton 873 instrument (Life Technologies, Carlsbad, CA, USA) using one ION PI chip. Sequence reads 874 were aligned to the human reference genome (Human GRCh37 (hg19) build) using Torrent 875 Mapping Alignment Program (TMAP) from the Torrent Suite (v5.0.2). The variants were 876 called using the Torrent Variant Caller (TVC) plugin (v5.0.2), and were annotated with the associated gene, location, protein position and amino acid changes, quality-score, coverage, 877 predicted functional consequences using SIFT⁸⁸, PolyPhen2⁸⁹, Grantham⁹⁰ prediction scores, 878 879 phyloP⁹¹ conservation scores, and 5000 genomes Minor Allele Frequencies. Variants were 880 filtered for common SNPs using the NCBI's "common and no known medical impacts" 881 database (ftp://ftp.ncbi.nlm.nih.gov/pub/clinvar/vcf GRCh37/), the Exome Aggregate 882 Consortium (ftp://ftp.broadinstitute.org/pub/ExAC release/release0.2/) and the Exome 883 Sequencing Project (http://evs.gs.washington.edu/EVS/). We next removed variants that 884 were present in greater than 1% of the previously in-house 478 sequenced samples. For the 885 Family 8 trio analysis, a total of 17.5 Gb, 14.8 Gb, and 14.6 Gb were sequenced with an 886 average read length of 183 bp, 175 bp, and 180bp for individuals IV:1, V:2, and V:4, 887 respectively. An average coverage of 212X, 183X, and 171X was achieved over the exome, 888 with 96% of bases covered at least 20X for each individual. A combined total of 46,723 889 variants were identified across protein-coding exons, UTRs, splice sites and flanking introns. 890 Additional filters were applied to retain variants that were homozygous in both probands and 891 heterozygous in the mother. A final set of 14 variants remained, of which only one was not a

892	common SNP, hg19: chr14:23571855 C>G, which corresponds to a TDT c.806G>C;
893	p.C269S mutation. Using the same method, we identified a homozygous TDT mutation in the
894	two probands in Family 9 (TDT c.1202_1204delTCT ; p.Phe401del) and in the proband of
895	Family 10 (TDT c.1144delG ; p.Q381fsX9/splicing defects). Subsequently, relatives with
896	available gDNA samples were tested for variant segregation analysis.

- 897 Data availability
- The data that support the findings of this study are available from the corresponding author upon reasonable request.

901 Acknowledgments

902 We are grateful to all members of the Reversade laboratory for support. We thank Ray 903 DUNN (NTU-LKC, Singapore) for the gift of the zebrafish lefty 1/2, spaw and insulin plasmids 904 for in situ hybridization experiments and critical feedback. We thank Vijay NARASIMHAN for 905 participating in the initial stages of the zebrafish study. E.S-R is supported by a NMRC Open 906 Fund - Young Individual Research Grant (OF-YIRG, #OFYIRG18May-0053). M.B. was 907 supported by DFG grants BL285/xx. T.O. was the recipient of a fellowship of the 908 Landesgraduiertenförderung Baden-Württemberg. B.R. is a fellow of the National Research 909 Foundation (NRF, Singapore) and Branco Weiss Foundation (Switzerland) and an EMBO 910 Young Investigator. This work was funded by a Strategic Positioning Fund for Genetic 911 Orphan Diseases and an inaugural A*STAR Investigatorship from the Agency for Science, 912 Technology and Research in Singapore.

913 Author contributions

914 E.S-R, T.O, M.B, P.B, and B.R designed the study. T.A-B, M.R, S.M, P.S, M.F, E.C, A.M, 915 L.D., G.C., S.DF, C.R-T, J-F.D, A.B, N.A, B.T, R.E, and P.B made clinical diagnoses and 916 collected clinical data and samples. Family 8 from T.A-B and M.R first allowed to identify 917 TDT as the causative gene. E.S-R, A.MdB, C.B, S.T, AYJ.N and B.V performed WES, 918 homozygosity mapping, high throughput cohort re-sequencing and sequencing analyses. 919 E.S-R, M.K, YL.C, WX.G, D.K, P.A, S.R and B.R performed and supervised the zebrafish 920 functional experiments. T.O and M.B performed and supervised the Xenopus functional 921 experiments. A.B and A.G performed and supervised the mouse experiments. V.R, B.E, F.E. 922 and B.V performed evolution genomics analyses. E.S-R and B.R wrote the manuscript with 923 input from S.R, M.B, and P.B.

924 Competing financial interest

925 The authors declare no competing financial interests.

926 References

927 1. Shiratori, H. & Hamada, H. TGFβ signaling in establishing left-right asymmetry. Semin.

928 *Cell Dev. Biol.* **32**, 80–84 (2014).

- 2. Zhang, H. T. & Hiiragi, T. Symmetry Breaking in the Mammalian Embryo. *Annu. Rev. Cell Dev. Biol.* 34, 405–426 (2018).
- Bier, E. & De Robertis, E. M. EMBRYO DEVELOPMENT. BMP gradients: A paradigm
 for morphogen-mediated developmental patterning. *Science* 348, aaa5838 (2015).
- 933 4. Sokol, S. Y. Wnt signaling and dorso-ventral axis specification in vertebrates. *Current*934 *Opinion in Genetics & Development* vol. 9 405–410 (1999).
- 5. Petersen, C. P. & Reddien, P. W. Wnt Signaling and the Polarity of the Primary Body
- 936 Axis. *Cell* **139**, 1056–1068 (2009).
- 937 6. Niehrs, C. Regionally specific induction by the Spemann–Mangold organizer. *Nature*938 *Reviews Genetics* 5, 425–434 (2004).
- 939 7. Blum, M. & Ott, T. Animal left-right asymmetry. *Curr. Biol.* 28, R301–R304 (2018).
- Shinohara, K. & Hamada, H. Cilia in Left-Right Symmetry Breaking. *Cold Spring Harb. Perspect. Biol.* 9, (2017).
- 942 9. Grimes, D. T. Making and breaking symmetry in development, growth and disease.
- 943 *Development* **146**, (2019).
- 944 10. Grimes, D. T. & Burdine, R. D. Left-Right Patterning: Breaking Symmetry to Asymmetric
 945 Morphogenesis. *Trends Genet.* 33, 616–628 (2017).
- 11. Sutherland, M. J. & Ware, S. M. Disorders of left-right asymmetry: heterotaxy and situs
 inversus. *Am. J. Med. Genet. C Semin. Med. Genet.* **151C**, 307–317 (2009).
- 12. Lin, A. E. et al. Laterality defects in the national birth defects prevention study (1998-
- 2007): birth prevalence and descriptive epidemiology. *Am. J. Med. Genet. A* **164A**,
- 950 2581–2591 (2014).
- 13. Mirra, V., Werner, C. & Santamaria, F. Primary Ciliary Dyskinesia: An Update on Clinical
- Aspects, Genetics, Diagnosis, and Future Treatment Strategies. *Front Pediatr* **5**, 135

953 (2017).

- 14. Zariwala, M. A., Omran, H. & Ferkol, T. W. The emerging genetics of primary ciliary
 dyskinesia. *Proc. Am. Thorac. Soc.* 8, 430–433 (2011).
- 956 15. Mohapatra, B. et al. Identification and functional characterization of NODAL rare variants
- 957 in heterotaxy and isolated cardiovascular malformations. *Hum. Mol. Genet.* 18, 861–871
 958 (2009).
- 16. Karkera, J. D. *et al.* Loss-of-function mutations in growth differentiation factor-1 (GDF1)
 are associated with congenital heart defects in humans. *Am. J. Hum. Genet.* **81**, 987–
 961 994 (2007).
- 962 17. Kosaki, R. *et al.* Left-right axis malformations associated with mutations in ACVR2B, the
 963 gene for human activin receptor type IIB. *Am. J. Med. Genet.* 82, 70–76 (1999).
- 18. Bamford, R. N. et al. Loss-of-function mutations in the EGF-CFC gene CFC1 are
- associated with human left-right laterality defects. *Nat. Genet.* **26**, 365–369 (2000).
- 19. Kosaki, K. et al. Characterization and Mutation Analysis of Human LEFTY A and LEFTY
- 967 B, Homologues of Murine Genes Implicated in Left-Right Axis Development. The
- 968 American Journal of Human Genetics **64**, 712–721 (1999).
- 20. Cristo, F. *et al.* Functional study of DAND5 variant in patients with Congenital Heart
- Disease and laterality defects. *BMC Med. Genet.* **18**, 77 (2017).
- 971 21. Sempou, E. & Khokha, M. K. Genes and mechanisms of heterotaxy: patients drive the
 972 search. *Curr. Opin. Genet. Dev.* 56, 34–40 (2019).
- 973 22. Perles, Z. *et al.* A human laterality disorder associated with recessive CCDC11 mutation.
 974 *J. Med. Genet.* 49, 386–390 (2012).
- 23. Narasimhan, V. et al. Mutations in CCDC11, which Encodes a Coiled-Coil Containing
- 976 Ciliary Protein, Causes Situs Inversus Due to Dysmotility of Monocilia in the Left-Right
- 977 Organizer. *Human Mutation* **36**, 307–318 (2015).
- 24. Vetrini, F. *et al.* Bi-allelic Mutations in PKD1L1 Are Associated with Laterality Defects in
- 979 Humans. Am. J. Hum. Genet. **99**, 886–893 (2016).
- 980 25. Gebbia, M. et al. X-linked situs abnormalities result from mutations in ZIC3. Nat. Genet.

981 **17**, 305–308 (1997).

- 982 26. Perles, Z. *et al.* A human laterality disorder caused by a homozygous deleterious
 983 mutation in MMP21. *J. Med. Genet.* 52, 840–847 (2015).
- 984 27. Guimier, A. *et al.* MMP21 is mutated in human heterotaxy and is required for normal left985 right asymmetry in vertebrates. *Nat. Genet.* 47, 1260–1263 (2015).
- 986 28. Akawi, N. et al. Discovery of four recessive developmental disorders using probabilistic
- genotype and phenotype matching among 4,125 families. *Nat. Genet.* 47, 1363–1369
 (2015).
- 989 29. Gros, J., Feistel, K., Viebahn, C., Blum, M. & Tabin, C. J. Cell movements at Hensen's
- 990 node establish left/right asymmetric gene expression in the chick. *Science* 324, 941–944
 991 (2009).
- 30. Blum, M., Feistel, K., Thumberger, T. & Schweickert, A. The evolution and conservation
 of left-right patterning mechanisms. *Development* 141, 1603–1613 (2014).
- 31. Yao, C., Donelson, J. E. & Wilson, M. E. The major surface protease (MSP or GP63) of

Leishmania sp. Biosynthesis, regulation of expression, and function. *Mol. Biochem.*

- 996 *Parasitol.* **132**, 1–16 (2003).
- 32. Petrovski, S. et al. Whole-exome sequencing in the evaluation of fetal structural
- anomalies: a prospective cohort study. *Lancet* **393**, 758–767 (2019).
- 33. Aamar, E. & Dawid, I. B. Sox17 and chordin are required for formation of Kupffer's
- vesicle and left-right asymmetry determination in zebrafish. *Dev. Dyn.* 239, 2980–2988
 (2010).
- 1002 34. Yu, X., Ng, C. P., Habacher, H. & Roy, S. Foxj1 transcription factors are master

regulators of the motile ciliogenic program. *Nat. Genet.* **40**, 1445–1453 (2008).

- 35. Stubbs, J. L., Oishi, I., Izpisúa Belmonte, J. C. & Kintner, C. The forkhead protein Foxj1
 specifies node-like cilia in Xenopus and zebrafish embryos. *Nat. Genet.* 40, 1454–1460
 (2008).
- 1007 36. Choksi, S. P., Babu, D., Lau, D., Yu, X. & Roy, S. Systematic discovery of novel ciliary
 1008 genes through functional genomics in the zebrafish. *Development* 141, 3410–3419

1009 (2014).

- 1010 37. Maisonneuve, C. et al. Bicaudal C, a novel regulator of Dvl signaling abutting RNA-
- processing bodies, controls cilia orientation and leftward flow. *Development* 136, 3019–
 3030 (2009).
- 1013 38. Beckers, A., Alten, L., Viebahn, C., Andre, P. & Gossler, A. The mouse homeobox gene
- 1014 Noto regulates node morphogenesis, notochordal ciliogenesis, and left right patterning.
 1015 *Proc. Natl. Acad. Sci. U. S. A.* **104**, 15765–15770 (2007).
- 1016 39. Huang, C.-J., Tu, C.-T., Hsiao, C.-D., Hsieh, F.-J. & Tsai, H.-J. Germ-line transmission of
- 1017 a myocardium-specific GFP transgene reveals critical regulatory elements in the cardiac
- 1018 myosin light chain 2 promoter of zebrafish. *Dev. Dyn.* **228**, 30–40 (2003).
- 1019 40. Szenker-Ravi, E. *et al.* RSPO2 inhibition of RNF43 and ZNRF3 governs limb
- development independently of LGR4/5/6. *Nature* **557**, 564–569 (2018).
- 1021 41. Blum, M. *et al.* Xenopus, an ideal model system to study vertebrate left-right asymmetry.
- 1022 Dev. Dyn. 238, 1215–1225 (2009).
- 1023 42. Hamada, H. Left-Right Asymmetry. *Mouse Development* 55–73 (2002).
- 43. Logan, M., Pagán-Westphal, S. M., Smith, D. M., Paganessi, L. & Tabin, C. J. The
- 1025 transcription factor Pitx2 mediates situs-specific morphogenesis in response to left-right
- asymmetric signals. *Cell* **94**, 307–317 (1998).
- 44. Yoshioka, H. *et al.* Pitx2, a bicoid-type homeobox gene, is involved in a lefty-signaling
 pathway in determination of left-right asymmetry. *Cell* **94**, 299–305 (1998).
- 45. Ryan, A. K. *et al.* Pitx2 determines left-right asymmetry of internal organs in vertebrates. *Nature* **394**, 545–551 (1998).
- 1031 46. Campione, M. et al. The homeobox gene Pitx2: mediator of asymmetric left-right
- signaling in vertebrate heart and gut looping. *Development* **126**, 1225–1234 (1999).
- 47. Schweickert, A. *et al.* The nodal inhibitor Coco is a critical target of leftward flow in
 Xenopus. *Curr. Biol.* 20, 738–743 (2010).
- 1035 48. Nakamura, T. et al. Fluid flow and interlinked feedback loops establish left-right
- asymmetric decay of Cerl2 mRNA. *Nat. Commun.* **3**, 1322 (2012).

- 1037 49. Skoog, T. et al. MMP-21 is expressed by macrophages and fibroblasts in vivo and in
- 1038 culture. *Exp. Dermatol.* **15**, 775–783 (2006).
- 1039 50. Ahokas, K. et al. Matrix metalloproteinase-21, the human orthologue for XMMP, is
- 1040 expressed during fetal development and in cancer. *Gene* **301**, 31–41 (2002).
- 1041 51. Ahokas, K. et al. Matrix metalloproteinase-21 is expressed epithelially during
- 1042 development and in cancer and is up-regulated by transforming growth factor-beta1 in
- 1043 keratinocytes. *Lab. Invest.* **83**, 1887–1899 (2003).
- Skoog, T. *et al.* Matrix metalloproteinase-21 expression is associated with keratinocyte
 differentiation and upregulated by retinoic acid in HaCaT cells. *J. Invest. Dermatol.* 129,
 119–130 (2009).
- 1047 53. Wu, T. *et al.* Increased MMP-21 expression is associated with poor overall survival of 1048 patients with gastric cancer. *Med. Oncol.* **30**, 323 (2013).
- 54. Zhang, J. *et al.* Overexpression of MMP21 and MMP28 is associated with gastric cancer
 progression and poor prognosis. *Oncol. Lett.* **15**, 7776–7782 (2018).
- 1051 55. Van Wart, H. E. & Birkedal-Hansen, H. The cysteine switch: a principle of regulation of
- 1052 metalloproteinase activity with potential applicability to the entire matrix
- 1053 metalloproteinase gene family. Proc. Natl. Acad. Sci. U. S. A. 87, 5578–5582 (1990).
- 1054 56. Field, S. et al. Pkd111 establishes left-right asymmetry and physically interacts with
- 1055 Pkd2. Development **138**, 1131–1142 (2011).
- 57. Bell, E. Cell fate specification and competence by Coco, a maternal BMP, TGFbeta and
 Wnt inhibitor. *Development* 130, 1381–1389 (2003).
- 1058 58. Piccolo, S. et al. The head inducer Cerberus is a multifunctional antagonist of Nodal,
- 1059 BMP and Wnt signals. *Nature* **397**, 707–710 (1999).
- 1060 59. Lee, H. X., Ambrosio, A. L., Reversade, B. & De Robertis, E. M. Embryonic dorsal-
- 1061 ventral signaling: secreted frizzled-related proteins as inhibitors of tolloid proteinases.
- 1062 *Cell* **124**, 147–159 (2006).
- 1063 60. Reversade, B. & De Robertis, E. M. Regulation of ADMP and BMP2/4/7 at opposite
- 1064 embryonic poles generates a self-regulating morphogenetic field. *Cell* **123**, 1147–1160

1065 (2005).

1092

- 1066 61. Jacob, F. & Monod, J. Genetic regulatory mechanisms in the synthesis of proteins. *J.*1067 *Mol. Biol.* 3, 318–356 (1961).
- 1068 62. Niehrs, C. & Pollet, N. Synexpression groups in eukaryotes. *Nature* 402, 483–487
 1069 (1999).
- 1070 63. Danilchik, M. V., Brown, E. E. & Riegert, K. Intrinsic chiral properties of the Xenopus egg
 1071 cortex: an early indicator of left-right asymmetry? *Development* 133, 4517–4526 (2006).
- 1072 64. Blum, M., Schweickert, A., Vick, P., Wright, C. V. E. & Danilchik, M. V. Symmetry
- 1073 breakage in the vertebrate embryo: when does it happen and how does it work? *Dev.*
- 1074 *Biol.* **393**, 109–123 (2014).
- 1075 65. Almagro Armenteros, J. J. *et al.* SignalP 5.0 improves signal peptide predictions using
 1076 deep neural networks. *Nat. Biotechnol.* **37**, 420–423 (2019).
- 1077 66. Sirota, F. L. *et al.* Beware of moving targets: reference proteome content fluctuates
 1078 substantially over the years. *J. Bioinform. Comput. Biol.* **10**, 1250020 (2012).
- 1079 67. Rouillard, A. D. et al. The harmonizome: a collection of processed datasets gathered to
- serve and mine knowledge about genes and proteins. *Database* **2016**, (2016).
- 1081 68. Sievers, F. *et al.* Fast, scalable generation of high-quality protein multiple sequence
- alignments using Clustal Omega. *Mol. Syst. Biol.* **7**, 539 (2011).
- 1083 69. Abdelkhalek, H. B. *et al.* The mouse homeobox gene Not is required for caudal
- 1084 notochord development and affected by the truncate mutation. *Genes & Development*1085 **18**, 1725–1736 (2004).
- 1086 70. Stauber, M. *et al.* Identification of FOXJ1 effectors during ciliogenesis in the foetal
- respiratory epithelium and embryonic left-right organiser of the mouse. *Dev. Biol.* 423,
 170–188 (2017).
- 1089 71. Westerfield, M. *The Zebrafish Book: A Guide for the Laboratory Use of Zebrafish*1090 (*Brachydanio Rerio*). (University of Oregon Press, 1989).
- 1091 72. Jao, L.-E., Wente, S. R. & Chen, W. Efficient multiplex biallelic zebrafish genome editing

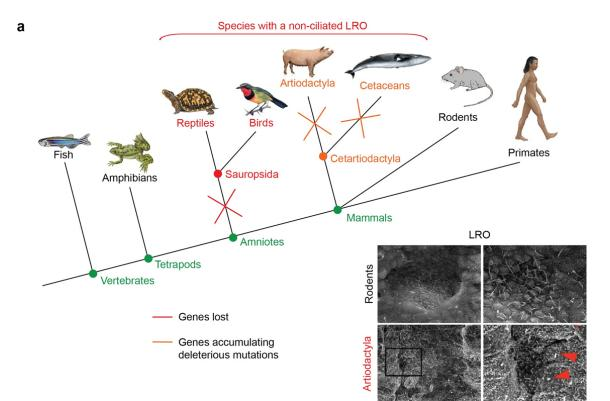
using a CRISPR nuclease system. Proc. Natl. Acad. Sci. U. S. A. 110, 13904–13909

1093 (2013).

- Thisse, C. & Thisse, B. High-resolution in situ hybridization to whole-mount zebrafish
 embryos. *Nat. Protoc.* **3**, 59–69 (2008).
- 1096 74. Moreno-Mateos, M. A. *et al.* CRISPRscan: designing highly efficient sgRNAs for
- 1097 CRISPR-Cas9 targeting in vivo. *Nat. Methods* **12**, 982–988 (2015).
- 1098 75. Nakayama, T. *et al.* Cas9-based genome editing in Xenopus tropicalis. *Methods* 1099 *Enzymol.* 546, 355–375 (2014).
- 1100 76. Hsiau, T. *et al.* Inference of CRISPR Edits from Sanger Trace Data.
- 1101 doi:10.1101/251082.
- 1102 77. Belo, J. A. *et al.* Cerberus-like is a secreted factor with neutralizing activity expressed in
- the anterior primitive endoderm of the mouse gastrula. *Mech. Dev.* **68**, 45–57 (1997).
- 1104 78. Schweickert, A. *et al.* Cilia-driven leftward flow determines laterality in Xenopus. *Curr.*1105 *Biol.* **17**, 60–66 (2007).
- 79. Rueden, C. T. *et al.* ImageJ2: ImageJ for the next generation of scientific image data. *BMC Bioinformatics* 18, 529 (2017).
- 80. Sbalzarini, I. F. & Koumoutsakos, P. Feature point tracking and trajectory analysis for
 video imaging in cell biology. *J. Struct. Biol.* **151**, 182–195 (2005).
- 1110 81. R Core Team. *R: A language and Environment for Statistical Computing*. https://www.R1111 project.org/ (2017).
- 82. Bahlo, M. & Bromhead, C. J. Generating linkage mapping files from Affymetrix SNP chip
 data. *Bioinformatics* 25, 1961–1962 (2009).
- 1114 83. Smith, K. R. *et al.* Reducing the exome search space for mendelian diseases using
- 1115 genetic linkage analysis of exome genotypes. *Genome Biol.* **12**, R85 (2011).
- 1116 84. Abecasis, G. R., Cherny, S. S., Cookson, W. O. & Cardon, L. R. GRR: graphical
- representation of relationship errors. *Bioinformatics* **17**, 742–743 (2001).
- 1118 85. Abecasis, G. R., Cherny, S. S., Cookson, W. O. & Cardon, L. R. Merlin--rapid analysis of
- dense genetic maps using sparse gene flow trees. *Nat. Genet.* **30**, 97–101 (2002).
- 1120 86. Thiele, H. & Nürnberg, P. HaploPainter: a tool for drawing pedigrees with complex

- 1121 haplotypes. *Bioinformatics* **21**, 1730–1732 (2005).
- 1122 87. Lindner, T. H. & Hoffmann, K. easyLINKAGE: a PERL script for easy and automated
 1123 two-/multi-point linkage analyses. *Bioinformatics* 21, 405–407 (2005).
- 1124 88. Kumar, P., Henikoff, S. & Ng, P. C. Predicting the effects of coding non-synonymous
- variants on protein function using the SIFT algorithm. *Nat. Protoc.* **4**, 1073–1081 (2009).
- 1126 89. Adzhubei, I. A. *et al.* A method and server for predicting damaging missense mutations.
- 1127 Nat. Methods **7**, 248–249 (2010).
- 90. Grantham, R. Amino acid difference formula to help explain protein evolution. *Science*1129 185, 862–864 (1974).
- 1130 91. Pollard, K. S., Hubisz, M. J., Rosenbloom, K. R. & Siepel, A. Detection of nonneutral
- substitution rates on mammalian phylogenies. *Genome Res.* **20**, 110–121 (2010).
- 1132 92. Follit, J. A. *et al.* Arf4 is required for Mammalian development but dispensable for ciliary
- assembly. *PLoS Genet.* **10**, e1004170 (2014).

1136 **Figures and legends**

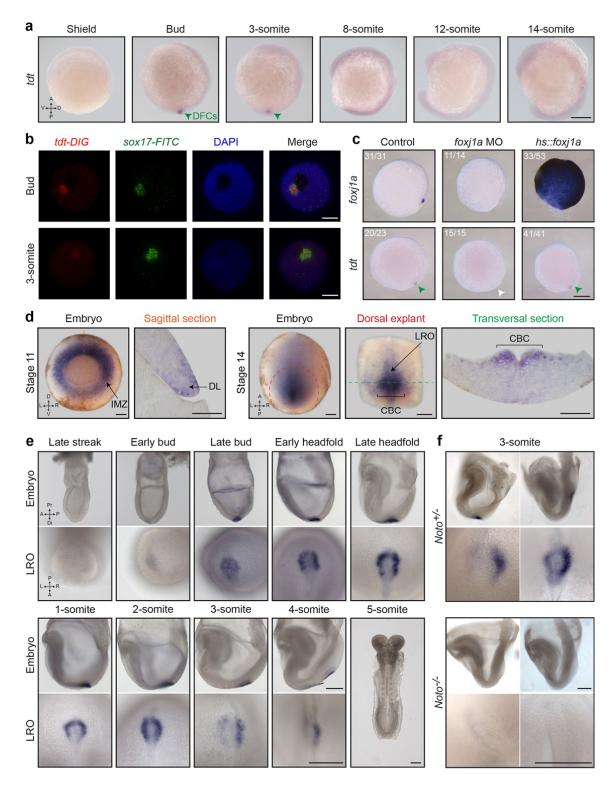


b

N									
	Gene	Protein	Signal	Present in	species with	Role in left-	right asymmetry	ОМІМ	
	Gene	rotein	peptide	a ciliated node	an unciliated node	in mouse	in human		
	TDT	Tout-de-travers	+	+	-	n.d.	this manuscript	n.d.	
	ALED	Alendroit	+	+	-	Cecilia Lo laboratory, MGI	(Petrovski S et al., 2019)	n.d.	
	MMP21	Matrix metalloprotease 21	+	+	-	(Guimier A et al., 2015)	(Guimier A et al., 2015; Perles et al., 2015; Akawi et al., 2015)	HTX7, 616749	
	PKD1L1	Polycystin-1, like 1	+	+	-	(Vogel P <i>et al.,</i> 2010 ; Field S <i>et al.,</i> 2011)	(Vetrini F et al., 2016)	HTX8, 617205	
	DAND5	DAN domain family member 5	+	+	-	(Marques S et al., 2004)	(Cristo et al., 2017)	n.d.	
	NODAL	Nodal	+	+	+	(Brennan J et al., 2002)	(Mohaptra B et al., 2009)	HTX5, 601265	
	GDF1	Embryonic growth/differentiation factor 1	+	+	+	(Rankin CT et al., 2000)	(Karkera JD <i>et al.,</i> 2007; Kaasinen E <i>et al.,</i> 2010)	CHTD6, 613854; RAI, 208530	
	ACVR2B	Activin receptor type 2B	+	+	+	(Oh SP et al., 1997)	(Kosaki R et al., 1999)	HTX4, 602730	
	CFC1	Cryptic	+	+	+	(Yan YT <i>et al.,</i> 1999; Gaio U <i>et al.,</i> 1999)	(Bamford RN et al., 2000)	HTX2, 605194	
	LEFTY2	Left-right determination factor 2	+	+	+	(Meno C et al., 2001)	(Kosaki K <i>et al.,</i> 1999)	n.d.	
С									
C		1 2 3 4	5	[6]	7 - 8	9-10-11 - 12	2202	Chr.14	
	_								
	TDT 1-	SP		catalytic Iomain	С	ysteine-rich domain	тм	-733	
F	igure 1	E. Szenker-Ravi <i>et</i>	al (2020)					
			, (<i>i</i>)					

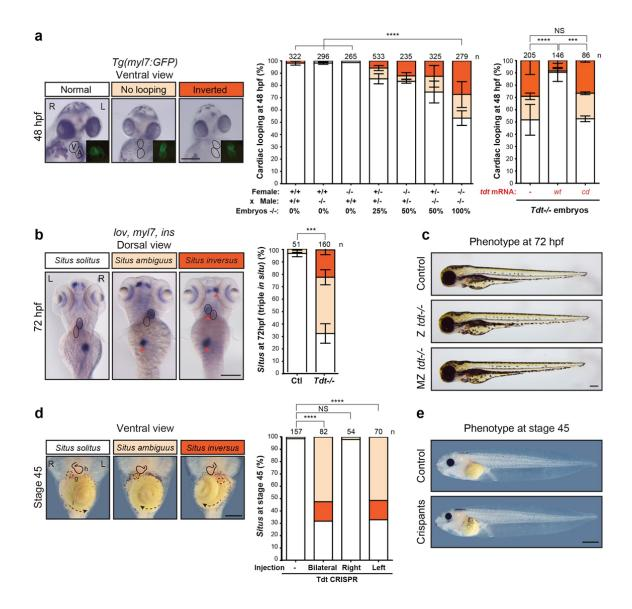
E. Szenker-Ravi et al., (2020)

Figure 1: Identification of 5 genes that are mutated or lost in species with a non-1138 ciliated LRO. (a) Simplified evolutionary tree of vertebrate species. Groups of species with a 1139 1140 ciliated LRO (black) or a non-ciliated LRO (red and orange) are outlined. Red crosses indicate where genes specific to the function of ciliated LROs have been lost and orange 1141 crosses where genes have accumulated deleterious mutations during evolution. 1142 Representative electron microscopy images of a ciliated LRO in a rodent (mouse)⁹² and a 1143 non-ciliated LRO in a cetartiodactyla (pig)²⁹ are shown. **(b)** Table indicating genes coding for 1144 1145 proteins with a signal peptide and either present or absent in species with a non-ciliated LRO. The references for a role in LR asymmetry and OMIM numbers, when available, are 1146 indicated. n.d.: not determined. (c) Genomic and protein structures of human TDT. Protein 1147 domains are highlighted: signal peptide (SP, gray), cysteine switch (brown), Zn²⁺ catalytic 1148 1149 domain (yellow) with a HExxH...H catalytic site (dark yellow) and a met-turn methionine (green), cysteine-rich domain (red), and transmembrane domain (TM, blue). Yellow line: 1150 1151 catalytic site, green line: met-turn. Chr.: chromosome.



1153 Figure 2 E. Szenker-Ravi et al., (2020)

Figure 2: Tdt is expressed in the LRO of zebrafish, Xenopus and mouse embryos. (a-c) 1155 Whole mount in situ hybridization in zebrafish embryos at indicated stages. (a) tdt expression 1156 1157 throughout development. The green arrowheads point to expression in the dorsal forerunner 1158 cells (DFCs). A: anterior, P: posterior, V: ventral, D: dorsal. Scale bar: 0.1 mm. (b) Double 1159 fluorescent in situ hybridization for tdt (DIG) and sox17 (FITC). Scale bars: 0.1 mm. (c) tdt and foxj1a expression in control, foxj1a morphants (MO) and transgenic hs::foxj1a heat-1160 1161 shocked zebrafish embryos at 90% epiboly. Arrowheads point to the DFCs with (green) or 1162 without (white) tdt expression. The numbers of analyzed embryos are indicated. Scale bar: 0.1 mm. (d) Whole mount in situ hybridization in Xenopus laevis embryos at indicated 1163 stages. Colored dotted lines indicate the respective sections. D: dorsal, V: ventral, L: left, R: 1164 1165 right, A: anterior, P: posterior, IMZ: involuting marginal zone, DL: dorsal lip of the blastopore, 1166 CBC: circumblastoporal collar, LRO: left-right organizer. Scale bar: 0.2 mm. (e-f) Whole 1167 mount in situ hybridization in mouse embryos at indicated stages. (e) Tdt expression in wildtype embryos throughout development. Whole embryos and zoomed-in pictures of the 1168 1169 LRO are shown. Pr: proximal, Di: distal, A: anterior, P: posterior. Scale bars: 0.2 mm. (f) Tdt expression in *Noto^{+/-}* and *Noto^{-/-}* mouse embryos. Two representative embryos and LROs for 1170 1171 each genotype are shown. Scale bars: 0.2 mm.



1173 Figure 3 E. Szenker-Ravi et al., (2020)

Figure 3: Zebrafish tdt' mutants and Xenopus tdt crispants present with LR 1175 **asymmetry defects. (a-c)** Zebrafish *tdf^{/-}* mutant embryos present with heterotaxy. (a) Left: 1176 1177 Cardiac looping of embryos can be visualized at 48 hpf by eye (delineated with a black line) 1178 or with the Tg(myl7:GFP) transgenic line (inserts). Scale bar: 0.1 mm. R: right, L: left, V: ventricle, A: atrium. Normal, no looping or inverted looping are classified in white, light 1179 orange and dark orange, respectively. Middle: The genotype of the parents (female and 1180 male) and the resulting percentage of tdt^{-} embryos are indicated for each type of cross 1181 under the graph. Cardiac looping of embryos at 48 hpf (percentage) is indicated. Right: tdf^{/-} 1182 1183 embryos were injected with wildtype (wt), or catalytic dead (cd, HExxH-AAxxA mutation) tdt

1184 mRNA at the one-cell stage, and cardiac looping was scored at 48 hpf. n: number of embryos analyzed from at least 3 independent experiments. NS: not significant, 1185 ****P<0.0001, ***P<0.001, Two-way ANOVA with Tukey test for multiple comparisons for the 1186 1187 normal looping condition. (b) Triple whole mount in situ hybridization for lov (brain), myl7 1188 (heart) and ins (pancreas) in 72 hpf embryos. Orange arrowheads indicate signals in the 1189 wrong position (heterotaxia). Representative pictures are shown. Situs ambiguus (light 1190 orange) indicates any intermediate state between situs solitus (white) and situs inversus 1191 (dark orange) with at least one organ in the wrong position. n: number of embryos analyzed 1192 from at least 3 independent experiments. ***P<0.001, Two-way ANOVA with Sidak test for 1193 multiple comparisons for the situs solitus condition. L: left, R: right, scale bar: 0.1 mm. (c) 1194 Absence of external phenotype in 72 hpf embryos. Z: zygotic, MZ: maternal zygotic, scale bar: 0.1 mm. (d-e) tdt is specifically required on the left side of the LRO for proper LR 1195 1196 asymmetry in Xenopus laevis. (d) Left: Representative images of the positioning of internal 1197 organs of stage 45 Xenopus larvae. The heart (h) and gallbladder (g) are delineated with black and dotted lines, respectively. The rotation of the intestine (i) is indicated with a dotted 1198 1199 arrow. Situs ambiguus (light orange) indicates any intermediate state between situs solitus 1200 (white) and situs inversus (dark orange) with at least one organ in the wrong position. Scale 1201 bar: 0.5 mm. Right: tdt CRISPR/Cas9 was injected bilaterally, on the right or on the left at the

4-cell stage and *situs* was analyzed at stage 45. n: number of embryos analyzed. NS: not
significant, ****P<0.0001, Chi-square test. (e) Absence of external phenotype at stage 45.
Scale bar: 1 mm.

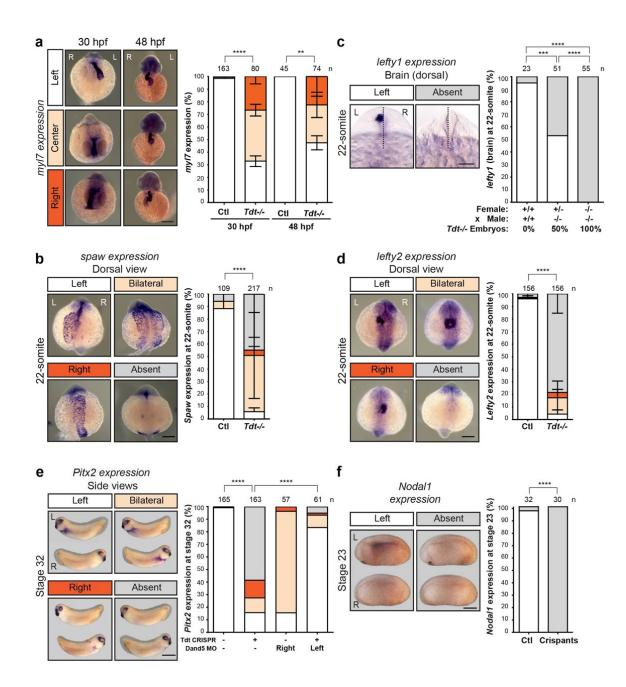
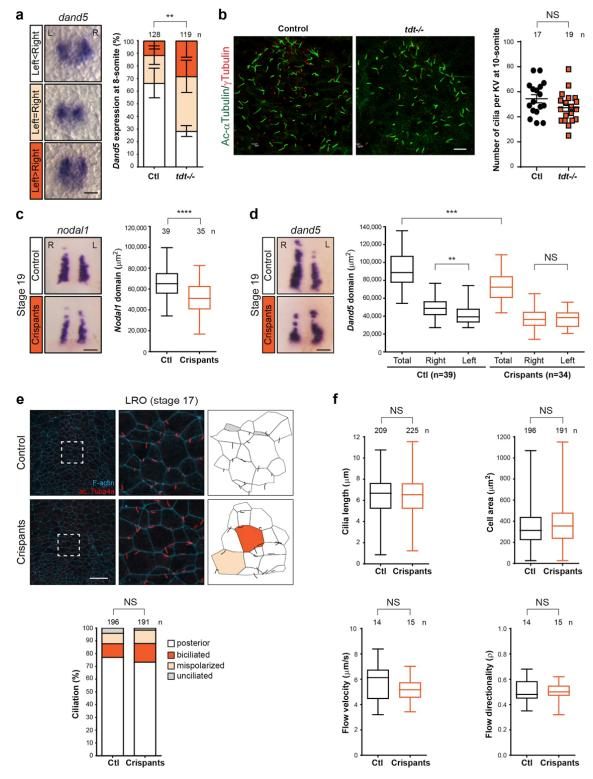


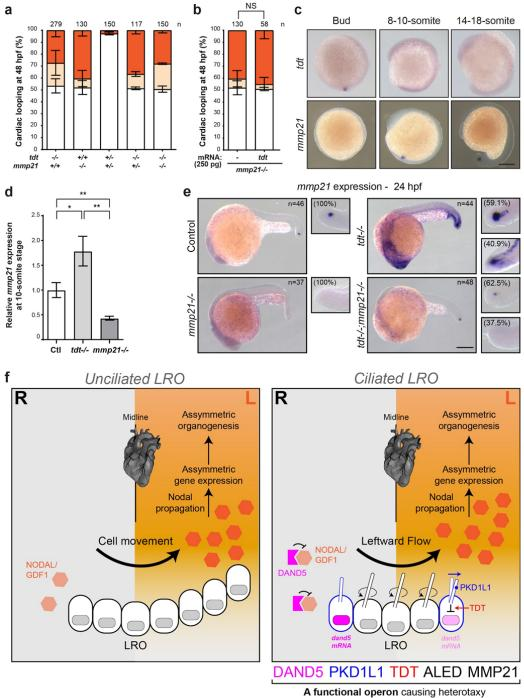


Figure 4: The Tdt requirement on the left side of the LRO can be bypassed by Dand5 1208 depletion. (a-d) Whole mount in situ hybridization in zebrafish embryos at indicated stages 1209 1210 and quantification. (a) my/7 expression in the heart with normal (left), no (center) or inverted 1211 (right) jogging / looping are classified in white, light orange and dark orange, respectively. ****P<0.0001, **P<0.01 Two-way ANOVA with Sidak test for multiple comparisons for the 1212 normal condition. spaw (b) and lefty2 (d) expression on the left, bilateral, on the right, or 1213 absent are classified in white, light orange, dark orange and gray, respectively. ****P<0.0001, 1214 1215 Two-way ANOVA with Sidak test for multiple comparisons for the expression on the left. (c) *lefty1* expression on the left or no expression are classified in white and gray, respectively. 1216 The genotype of the parents (female and male) and the resulting percentage of tdt^{-} embryos 1217 are indicated for each type of crosses under the graph. ****P<0.0001, ***P<0.001, Chi-1218 1219 square test. (e-f) Whole mount in situ hybridization in Xenopus laevis embryos at indicated stages and guantification. (e) Embryos were injected bilaterally at the 1- and 4-cell stage with 1220 1221 tdt CRISPR/Cas9 and dand5 morpholino (MO) on the right or on the left, respectively, as 1222 indicated. pitx2 expression on the left, bilateral, right or absent are classified in white, light orange, dark orange, and gray, respectively. ****P<0.0001, Fisher's exact test. (f) Embryos 1223 1224 were injected at the 1-cell stage with tdt CRISPR/Cas9. nodal1 expression on the left or no expression are classified in white and gray, respectively. ****P<0.0001, Fisher's exact test. 1225 1226 (a-f) L: left, R: right, scale bar: 0.1 mm. n: number of embryos analyzed from at least 3 1227 independent experiments.



1229 Figure 5 E. Szenker-Ravi et al., (2020)

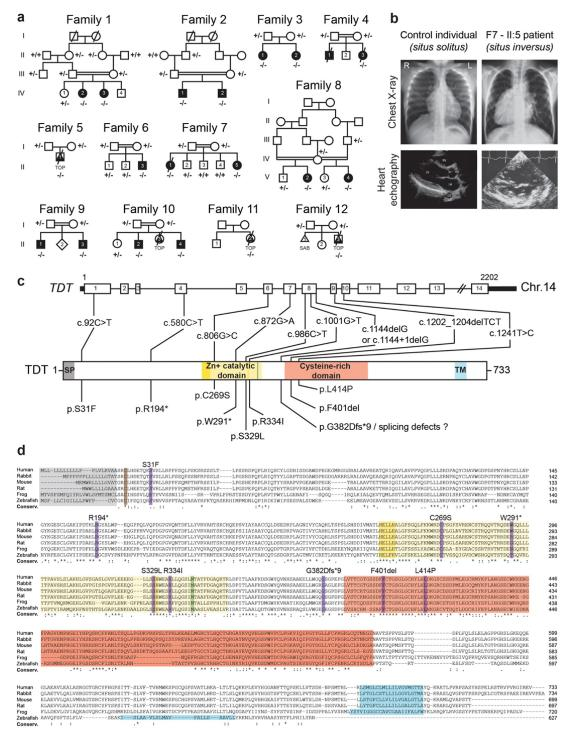
Figure 5: Tdt is required on the left side of the LRO for proper *dand5* downregulation 1231 downstream of leftward flow. (a-c) Analysis of dand5 expression and ciliogenesis in control 1232 (ctl) and tdt^{-} mutant zebrafish embryos. (a) dand5 expression at the 8-somite stage. 1233 1234 Stronger signal on the right is shown in white (normal condition), same intensity on both sides in light orange and stronger signal on the left in dark orange. **P<0.01, Two-way 1235 ANOVA with Sidak test for multiple comparisons for the normal condition. n= number of 1236 1237 embryos. L= left, R: right, scale bar: 0.05 mm. (b) Representative images of an 1238 immunofluorescence for acetylated- α Tubulin (green) and γ Tubulin (red) marking the axonemes and basal bodies of cilia, respectively, on KV at the 10-somite stage. Numbers of 1239 cilia per KV are plotted. NS: non-significant, unpaired t-test. n= number of embryos. KV: 1240 1241 Kupffer's vesicle, scale bar: 10 µm. (c-f) Analyses in Xenopus laevis control (ctl) and tdt 1242 crispants. (c-d) Expression of nodal1 (c) and dand5 (d) in control (white) and tdt crispants (dark orange) at stage 19. NS: non-significant, ****P<0.0001, ***P<0.001, **P<0.01, unpaired 1243 1244 t-test. n= number of embryos. R: right, L=left, scale bar: 0.1 mm. (e) Immunofluorescence on 1245 Xenopus LRO for acetylated- α -tubulin4a (red) and F-actin (cyan) marking the cilia and cell 1246 membrane, respectively. Cells with a single posterior-oriented cilium are shown in white, and 1247 cells that are bi-ciliated, unciliated or with a mispolorized cilium are represented in dark orange, gray and light orange, respectively. n= number of cells analyzed. NS: non-significant, 1248 1249 Chi-square test. LRO: left right organizer, scale bar: 50 µm. (f) Measurements of cilia length 1250 (n= number of cilia), cell area (n= number of cells), and flow velocity and directionality (n= 1251 number of embryos) of control (ctl) and tdt crispants LRO. NS: non-significant, unpaired t-1252 test.



when mutated in zebrafish, *Xenopus* and humans

1254 Figure 6 E. Szenker-Ravi et al., (2020)

Figure 6: TDT acts upstream of MMP21. (a-b) Cardiac looping of embryos visualized at 48 1257 hpf is classified as normal, no looping or inverted looping in white, light orange and dark 1258 1259 orange, respectively. The genotype of the embryos is indicated under the graph. n: number 1260 of embryos analyzed from at least 3 independent experiments. (a) Embryos with indicated genotype for *tdt* and *mmp21*. (b) *mmp21^{-/-}* embryos injected without or with 250 pg of *tdt* 1261 1262 mRNA. (c) Whole mount in situ hybridization for tdt and mmp21 in zebrafish embryos at 1263 indicated stages. DFCs: dorsal forerunner cells, KV: Kupffer's vesicle. Scale bar: 0.1 mm. (d) 1264 Real-time gPCR for *mmp21* relative to *actin* in zebrafish embryos of indicated genotype at the 10-somite stage. *P<0.05, **P<0.01, Two-way ANOVA with Tukey test for multiple 1265 comparisons. (e) Whole mount in situ hybridization for mmp21 in zebrafish embryos of 1266 1267 indicated genotype at the 24 hpf stage. The number of analyzed embryos is indicated and a 1268 zoom with expression in the tail region with percentages of embryos is shown. Scale bar: 0.1 mm. (f) Our working model proposes that TDT works in concert with at least 4 partner 1269 1270 proteins DAND5, PKD1L1, ALED and MMP21 to form an extracellular module needed to 1271 sense and propagate the NODAL/GDF1 signalling cascade on the left. R: right, L: left, LRO: 1272 left-right organizer, central (black) and lateral (blue) LRO cells are shown with their motile 1273 and immotile cilia, respectively.



1275 Figure 7 E. Szenker-Ravi et al., (2020)

Figure 7: Identification of recessive TDT mutations in patients with heterotaxy 1278 associated with congenital heart defects. (a) Pedigrees of twelve families with individuals 1279 1280 presenting with heterotaxy. The TDT genotype for available individuals are indicated. 1281 Squares, circles, diamonds and triangles denote males, females, unknown gender 1282 individuals and fetuses, respectively. Open and filled symbols are used for unaffected and affected family members, respectively, and deceased individuals are indicated by a diagonal 1283 1284 slash through the symbol. +: wildtype allele, -: mutant allele, TOP: termination of pregnancy, 1285 SAB: spontaneous abortion. (b) Chest X-ray and heart echography of a control individual and the F7-II:5 patient presenting with situs inversus associated with a double outlet right 1286 1287 ventricle of the heart. R: right, L: left. (c) Genomic and protein structures of human TDT. The 1288 position and nature of the identified mutations are indicated. TDT protein domains are 1289 highlighted: signal peptide (SP, gray), Zn+ catalytic domain (yellow), cysteine-rich domain 1290 (red), and transmembrane domain (TM, blue). Yellow line: catalytic site, green line: met-turn. Chr.: chromosome. (d) TDT proteins alignment highlighting the conservation of the affected 1291 1292 amino acids in patients with heterotaxy (purple). TDT protein domains are highlighted: signal 1293 peptide (gray), Zn+ catalytic domain (yellow), cysteine-rich domain (red), and 1294 transmembrane domain (blue). Brown C: cysteine switch, dark yellow amino acids: catalytic site (HExxH...H), green M: met-turn, purple: mutated amino acids. Conserv.: conservation. 1295 1296 Software used: Clustal Omega.

1297

1298

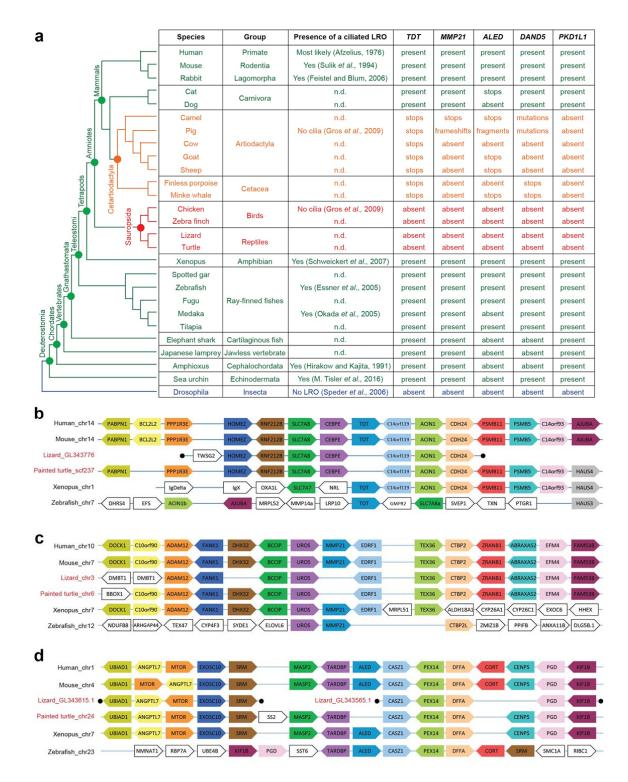
1299

1300

1301

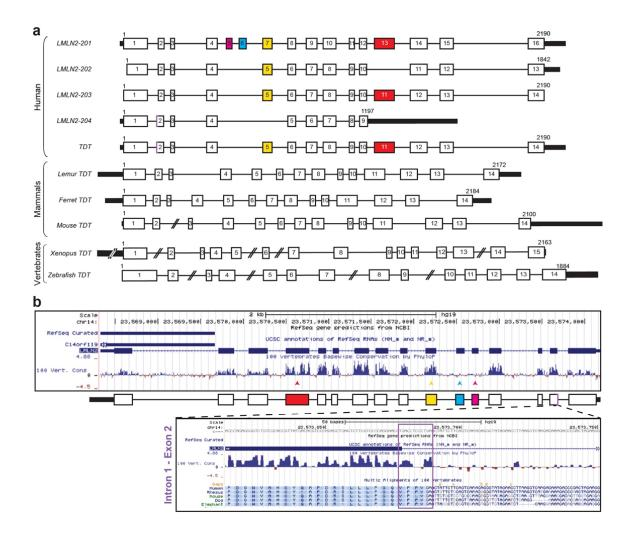
1303
 Table 1: Clinical characteristics of patients with biallelic TDT mutations.
 Abbreviations:
 1304 -: absence of phenotype, AS: aortic valvar stenosis; ASD: atrial septal defect; ASD-OP: atrial 1305 septal defect ostium primum type; CA: common atrium; CAVC: complete atrioventricular 1306 canal; CoA: Aortic coarctation; DIRV: double inlet right ventricle; DORV: double outlet right ventricle; IAA: interrupted aortic arch; IVC: inferior vena cava; n.d.: not determined; PA: 1307 1308 pulmonary atresia; PAPVC: partial anomalous pulmonary venous connection; PDA: patent 1309 ductus arteriosus; PFO: patent foramen ovale; PS: pulmonary stenosis; SVC: superior vena cava; TA: tricuspid valve atresia; TGA: transposition of the great arteries; TOP: termination of 1310 1311 pregnancy; VSD: ventricular septal defect.

1313 Supplementary figures and legends



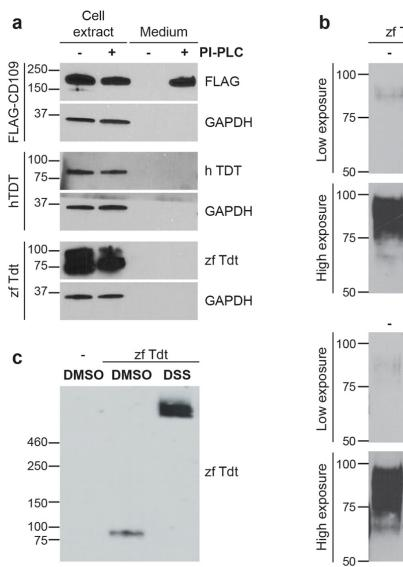
1314 Figure S1 E. Szenker-Ravi et al., (2020)

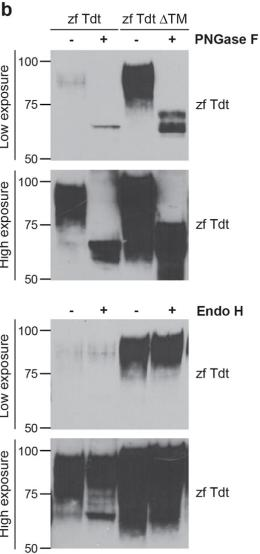
Figure S1: TDT, MMP21, ALED, DAND5 and PKD1L1 are specifically lost in species 1315 with a non-ciliated LRO. (a) Table indicating the presence of the TDT, MMP21, ALED, 1316 1317 DAND5 and PKD1L1 genes in metazoan species in relation to the presence or absence of a ciliated LRO. It is believed that a ciliated LRO evolved in deuterostomia (green), but cilia in 1318 the LRO disappeared in cetartiodactyla (orange) and sauropsida (red). LRO: Left-right 1319 1320 organizer, n.d.: not determined. (b-d) Representation of the TDT (b), MMP21 (c) and ALED 1321 (d) loci in representative jawed-vertebrates whose genomes have been sequenced, showing the loss of the 3 genes in lizards and turtles (reptilia). Block arrows represent genes with the 1322 1323 direction of arrows denoting transcriptional orientation. Orthologous genes are shown with the same colour. Black circles represent ends of scaffolds. 1324



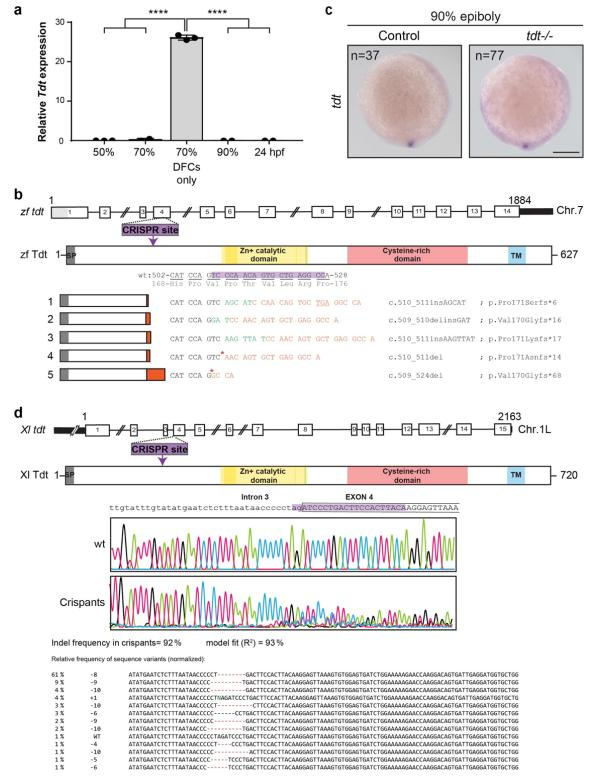
1325 Figure S2 E. Szenker-Ravi et al., (2020)

Figure S2: Genomic structure of TDT. (a) Genomic exon-intron structure of four distinct 1327 variants of human TDT (LMLN2) from Ensembl, and the predicted full length TDT as 1328 1329 compared to that of other primates and vertebrates as indicated. The alternative exons are color coded as follows: pink and blue exons are only present in LMLN2-201, yellow exon is 1330 missing in LMLN2-204 and red exon is missing in LMLN2-202. Full length human TDT 1331 corresponds to LMLN2-203 with three extra amino acids in the beginning of exon 2 (purple) 1332 that are present in LMLN2-204 (see b). The UTRs are highlighted in dark gray. (b) Genomic 1333 1334 region on the UCSC browser containing TDT with the conservation in vertebrates, showing that the pink and blue exons are not conserved while the yellow and red ones are highly 1335 conserved. A zoom in the intron1-exon2 junction region confirms the conservation of the 3 1336 1337 additional amino acids (purple box) present in LMLN2-204.



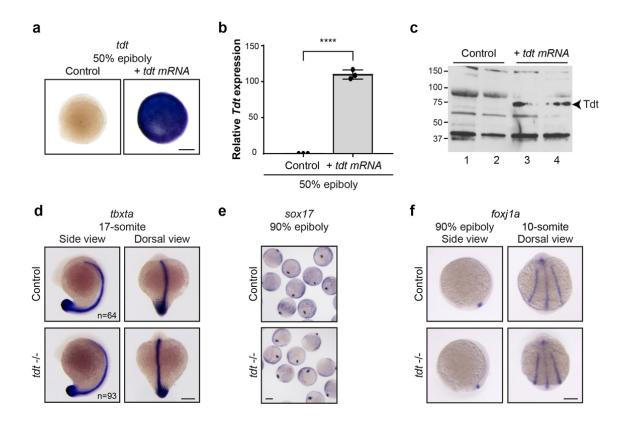


1339 Figure S3: TDT is post-translationally modified but not GPI-anchored. (a) Western blot 1340 using cell extracts and conditioned media of HEK293T cells transfected with human TDT, 1341 zebrafish Tdt or FLAG-CD109 and treated with or without PI-PLC. FLAG-CD109 serves as a 1342 positive control of a GPI-anchored protein. (b) Western blot using conditioned media from HEK293T cells transfected with zebrafish *Tdt* or zebrafish *Tdt* encoding a variant lacking the 1343 transmembrane domain (Δ TM) treated with or without PNGase F and Endo H, as indicated. 1344 (c) Western blot using conditioned media from HEK293T cells transfected with zebrafish Tdt 1345 and crosslinked in solution with DSS (a-c). Primary antibodies used are indicated, sizes are 1346 1347 in kDa.



1348 Figure S4 E. Szenker-Ravi et al., (2020)

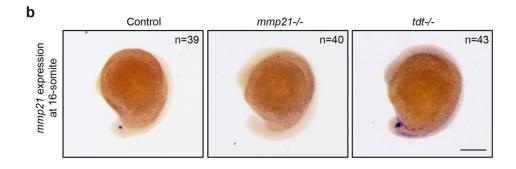
Figure S4: CRISPR-Cas9 knockout of Tdt in zebrafish and Xenopus laevis. (a) Real-time 1350 qPCR for tdt relative to actin in zebrafish embryos at indicated stages. tdt expression is only 1351 1352 detectable using RNA extracted from tissue at the dorsal posterior side containing the DFCs. ****P<0.0001, Two-way ANOVA with Tukey test for multiple comparisons. DFC: dorsal 1353 forerunner cells. n= number of embryos. (b) Depiction of genomic and protein structures of 1354 1355 zebrafish Tdt. The sequence used is XM 002662823 using a START codon located 168 nucleotides upstream of the original one (light gray). Tdt protein domains are highlighted: the 1356 1357 signal peptide (gray), the Zn+ catalytic domain (yellow), the cysteine-rich domain (red), and the transmembrane domain (blue). Yellow line: catalytic domain, green line: met-turn. The 1358 site and targeted sequence by the CRISPR gRNA is indicated in purple. Five different alleles 1359 1360 were obtained with indicated mutations (green: insertion, red star: deletion), all leading to a 1361 frameshift (orange) with an early stop codon (underlined for mutation 1). While all mutations lead to the same LR phenotype in the homozygous state, line 1 was used for further 1362 investigation. (c) Whole mount in situ hybridization for tdt in 90% epiboly control and tdf^{/-} 1363 1364 zebrafish embryos. Scale bar: 0.1 mm. (d) Depiction of genomic and protein structures of 1365 Xenopus laevis Tdt. A CRISPR gRNA was designed in the beginning of exon 4 (purple), leading to mutations with 92% efficiency. Chr.: chromosome, SP: signal peptide, TM: 1366 transmembrane domain, wt: wildtype, XI: Xenopus laevis. 1367



1368 Figure S5 E. Szenker-Ravi et al., (2020)

Figure S5: The absence of Tdt does not affect the DFCs or midline patterning. (a-c) Analysis of zebrafish embryos injected or not with *tdt* mRNA by whole mount *in situ* hybridization (a), real-time qPCR (b) and western blotting (c). Scale bar: 0.1 mm, ****P<0.0001, unpaired t-test. (d-f) Whole mount *in situ* hybridization in control and *tdt*^{-/-} zebrafish embryos for *tbxta* (d), *foxj1a* (e), and *sox17* (f) at indicated stages. Scale bars: 0.1 mm.

а	mmp21	21 1800 21 1 1 1 2 1 3 1 4 5 6 1 7 1 8 1 9 mm Chr.12 CRISPR site 1 ↓ 5 6 1 7 1 8 1 9 mm Site 599														
	Mmp21	SP	Prodomain	Peptidase domain	Hx 1	Hx 2	Hx 3 H	x 4								
				CG GAG CTG ATC ACT GAC												
	1		CAG G	CG GAG CTG ATC ACT GTC	TGT GGA	CAC GGA	CAC TGC A	CA G c.127_128insTCTGTGG ; p.Asp43Valfs*23								
	2		CAG G	CG GAG CTG ATC ACT GA	CAC TGC	ACA G		c.128_132delACACG ; p.Asp43Glyfs*19								
	3		CAG [*] C	TG ATC ACA CGG ACA CTG	CAC AG		c.112_1	17delGCGGAG+124_127delACTG ; p.Ala38Leufs*62								



1376 Figure S6 E. Szenker-Ravi et al., (2020)

1378 Figure S6: Generation of Mmp21 mutant zebrafish. (a) Depiction of genomic and protein 1379 structures of zebrafish Mmp21. MMP21 protein domains are highlighted: signal peptide 1380 (gray), prodomain (pink), peptidase domain (yellow) and hemopexin (hx) repeats (blue). The 1381 site and targeted sequence by the CRISPR gRNA is indicated in purple. F1 fish were a gift 1382 from Katsanis laboratory. Three different alleles were obtained with indicated mutations 1383 (green: insertion, red star: deletion), all leading to a frameshift (orange) with an early stop 1384 codon. While all mutations lead to the same LR phenotype in the homozygous state, line 3 was used for further investigation. (b) Whole mount in situ hybridization for mmp21 in 1385 1386 zebrafish embryos of indicated genotypes at the 16-somite stage. The numbers of analyzed embryos are indicated. Scale bar: 0.1 mm. 1387

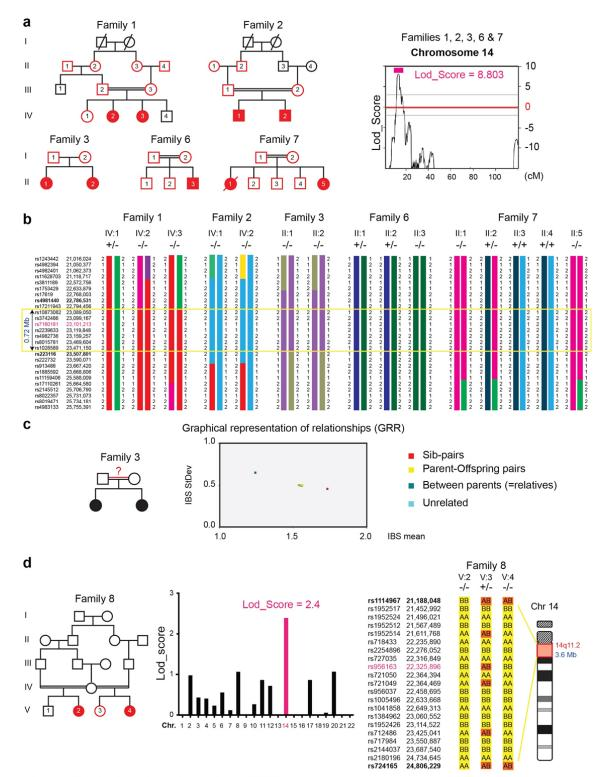


Figure S7 E. Szenker-Ravi et al., (2020)

Figure S7: Mapping analysis of 6 families with patients presenting with heterotaxy 1390 reveal a region of homozygosity on chr. 14. (a-b) Individuals of Families 1, 2, 3, 6 and 7 1391 1392 with red symbols in pedigrees were SNP genotyped. Genotypes were used for linkage analysis which revealed a common region of homozygosity for affected individuals on 1393 chromosome 14, including the genomic region of TDT, with a total Lod Score of 8.803. 1394 1395 Graphical representation obtained using Merlin Autosome. (b) Haplotypes obtained with Merlin and presented with Haplopainter revealed a common region of homozygosity on 1396 1397 chromosome 14g11.2 delimited by rs17211943 and rs223116 that is 0.72 Mb long. (c) 1398 Graphical representation of relationships (GRR) showing that parents of Family 3 are actually related. (d) Family 8 SNP genotyping of individuals V:2, V:3, V:4 (red in pedigree) reveal a 1399 1400 Lod Score max on chromosome 14q11.2 with SNP rs956163 (pink) for affected individuals. 1401 The region of homozygosity shared by V:2 and V:4 is 3.6 Mb long, delimited by rs1114967 1402 and rs724165.

- 1404 Table S1: List of the cases in the original cohort screened for *TDT* mutations.
- 1405 Table S2: List of genes with a S score above 1.
- 1406 Movie S1: Cilia movement in KV of a WT zebrafish embryo.
- 1407 Movie S2: Cilia movement in KV of a tdt' zebrafish embryo.
- 1408 Movie S3: Movement of endogenous particles in KV of a WT zebrafish embryo.
- 1409 Movie S4: Movement of endogenous particles in KV of a tdt^{-} zebrafish embryo.
- 1410 **Movies S1-S4:** 8-10 somite stage zebrafish embryos were dechorionated and mounted in
- 1411 2% low melting agarose, and KV were imaged with a 60 x water lens from the dorsal 1412 posterior end.
- 1413 Movie S5: Analysis of leftward flow in the LRO of *Xenopus* wildtype and *Tdt* crispants.
- 1414 Dorsal explants were prepared and fluorescent micro beads added. Time-lapse movies were
- 1415 captured at 2 fps and transformed to gradient-time-trails (GTTs). GTT movies play at about
- 1416 10 x real time and display bead transport from the right to the left side of the LRO. Note that
- velocity and directionality of bead transport were identical in WT (left) and *Tdt* crispant (right)
- 1418 specimens.

	Family 1		Family 2		Family 3		Family 4		Family 5	Family 6	Family 7		Family 8		Family 9		Family 10				
																			Family 11		
	IV:2	IV:3	IV:1	IV:2	II:1	II:2	II:1	II:3	II:1	II:3	II :1	II :5	V:2	V:4	II:1	II:3	II:2	II:3	II:4	II:2	II:3
Gender	female	female	male	male	female	female	male	female	male	male	female	female	female	female	male	male	male	female	male	female	male
Year of birth	1989	1991	1987	1992	1984	1989	1985	1990	2014	1991	1983	1992	1989	2006	1997	2000	2005	2007	2009	2015	2015
Age at death	alive	alive	n.d.	n.d.	alive	alive	deceased (2 months)	deceased (10 years)	TOP	n.d.	deceased (9 years)	alive	alive	alive	n.d.	n.d.	alive	TOP	alive	TOP	TOP
Country of origin	Т	urkey	Τu	urkey	Italy (So	uth Tyrol)	Т	urkey	France	Turkey	Τι	urkey	Fra	ance	Let	anon		Lebanon		France	France
Consanguineous parents		yes	у	/es	not initially	y reported		/es	not reported	yes	<u> </u>	/es	y	yes	y	'es		yes		not reported	no
<i>TDT</i> DNA	c.98	36C>T	c.92	2C>T	c.872		c.10	01G>T	c.92C>T	c.1241T>C	c.10	01G>T	c.80	06C>T	c.1202_1	204deITCT		c.1144delG / c.1144+1del0	G	c.92C>T	c.92C>T (paternal) & c.580C>T (maternal)
TDT protein	p.Ser329Leu p.Ser31Phe		er31Phe	p.Trp291*		p.Arg334lle		p.Ser31Phe	p.Leu414Pro	p.Arg334lle		p.Cys269Ser		p.Phe401del		p.Gly382Aspfs*8 / p.? (splicing defects?)		p.Ser31Phe	p.Ser31Phe & p.Arg194*		
Mutation status	s homozygous		homo	homozygous homozygo		zygous	ous no DNA available (parents heterozygous) homozygous		homozygous	homozygous	homozygous homozygous		homozygous		homozygous homozygo		homozygous	no DNA available (parents heterozygous)	homozygous	homozygous	compound heterozygous
Heterotaxy	Situs inversus	Situs inversus	Abdominal situs ambiguus	Situs solitus	Situs solitus	Situs solitus	Situs solitus	Situs ambiguus	Left isomerism	Situs inversus	Situs solitus	Situs inversus	Situs inversus	Situs inversus	Situs solitus	Situs solitus	Situs inversus	Situs solitus	Situs inversus	Situs ambiguus	Situs ambiguus
Position of organs	Complete reversal	Complete reversal	Midline liver	Isolated dextrocardia	Isolated dextrocardia	Isolated dextrocardia	Normal	Dextrocardia, Asplenia midline liver (abdomina right isomerism)	a, Pulmonary and atrial left al isomerism, Polysplenia, absent pancreatic tail	Complete reversal	Normal	Complete reversal	Complete reversal	Complete reversal	Isolated dextrocardia	Isolated dextrocardia	Complete reversal	Normal	Complete reversal	Intestinal malrotation, polyspenia, left pulmonary isomerism	Intestinal malrotation, polysplenia, annular pancreas, left pulmonary isomerism
Cardiac phenotypes	VSD, right SVC to the coronary sinus	Congenitally corrected TGA,VSD, PA	Left IVC with hemiazygous continuation, hepatic veir abnormality,CA, CAVC, DORV, subvalvular pulmonary stenosis	ASD, congenitally corrected TGA, PA, PDA	PFO, DIRV, PA, PDA, right aortic arch	ASD, discordant atrioventricular connection, subaortic VSD, vavular and subvavular PS, PDA	DORV, PDA, IAA after left subclavian artery	Congenitally corrected TGA, ASD-OP, TA, Co PDA	d A, PAPVC, CAVC, left ventricle hypoplasia, AS, aortic arch hypoplasia	Common atrium, CAVC	Absent IVC with azygos continuation to right SVC left SVC to coronary sinus, discordant atrio- ventricular connection	Right SVC to coronary	no CHD	DORV	DORV, PS	no CHD	Left SVC, Common atrium, CAVC, Single Ventricle right type, PS, TGA	CAVC, Single Ventricle left type, hypoplastic pulmonary artery	CA, CAVC, Single ventricle right type, Pulmonary stenosis	Left SVC to the corona sinus, CAVC, single coronary artery, hypoplastic aortic arch	Absent IVC with hemi- azygos continuation, PAPVC, CA with appendages left isomerism, single ventricle, double aortic arch
Others	n.a.	Pace maker for Atrioventricular block (1998)	n.a.	n.a.	n.a.	n.a.	n.a.	n.a.	Microretrognathism, low- set ears, receding forehead, 11 rib pairs	n.a.	n.a.	n.a.	n.a.	Right kidney: dilated Left kidney: hyperechoic	n.a.	n.a.	n.a.	n.a.	n.a.	Dolichocephaly, hypertelorism	n.a.

Table 1 Szenker-Ravi *et al. ,* (2020)

Abbreviations: AS: a ortic valvar stenosis; ASD: atrial septal defect; ASD-OP: atrial septal defect; ot: common atrium; CAVC: complete atrioventricle; IAA: interrupted aortic arch; IVC: inferior vena cava; n.a.: not applicable; n.d.: not determined; PA: pulmonary atresia; PAPVC: partial anomalous pulmonary stenosis; SVC: superior vena cava; n.a.: not applicable; n.d.: not determined; PA: pulmonary atresia; PAPVC: partial anomalous pulmonary atresia; PAPVC: partial anomalous pulmonary stenosis; SVC: superior vena cava; n.a.: not applicable; n.d.: not determined; PA: pulmonary stenosis; SVC: superior vena cava; n.a.: not applicable; n.d.: not determined; PA: pulmonary atresia; PAPVC: partial anomalous pulmonary atres